ioMosaic®

*Minimizing risk. Maximizing potential.®*

# Kinetics Development with RSM. Part 1: Acetic Anhydride-Methanol Reaction

## Process Safety and Risk Management Practices

An ioMosaic White Paper

**Date:** September 4, 2024

# How Do You Develop a Kinetic Model in Process Safety Office® SuperChems™?

A kinetic model is required for upset scenarios with runaway chemical reactions that are analyzed dynamically through SuperChems™. Kinetic parameters for these chemical reactions are usually determined by trial and error, one variable at a time. The simplest case requires two parameters, the pre-exponential factor and the activation energy. Even this unpretentious condition presents obstacles. When fixing the pre-exponential factor to determine the activation energy or vice-versa, one is optimized for the fixed value of the other, which most likely is not the real optimum. Neither parameter is optimized in this manner.

It is virtually impossible to optimize kinetic parameters by trial and error when two or more factors are present, so it makes sense to consider an alternative technique. One effective method is Experimental Design, a statistical technique that simultaneously identifies the optimum of all model factors under consideration. An experimental design organizes, conducts, and interprets the results for the best outcome based on the smallest number of trials.

The word trial usually refers to experiments. When developing a kinetic model, a trial represents a SuperChems™ run with kinetic parameters that are part of the design. The typical experimental design works with squares, cubes, or hypercubes, depending on the number of input variables or predictors. A multi-dimensional cubic design is much better than trial and error. However, there is a superior experimental design technique that can be applied to establish kinetic parameters, known as Response Surface Methodology (RSM) [1], carried out with a Central Composite Design (CCD) [2].

RSM is a collection of mathematical and statistical techniques for modeling and analyzing complex relationships between kinetic parameters (predictors) and kinetic rates (responses or control variables).

This white paper employs a known chemical reaction to provide the background for kinetic development with RSM. It is the exothermic reaction of acetic anhydride with methanol, yielding methyl acetate and acetic acid. The goal is to generate kinetic parameters for SuperChems™ dynamic simulations involving runaway reactions.

*“We cannot effectively develop kinetic parameters for a runaway chemical reaction by trial and error.”*

## The Chemical Reaction of Acetic Anhydride and Methanol

The overall reaction of acetic anhydride with methanol can be summarized as follows:

Without consideration for autocatalysis:

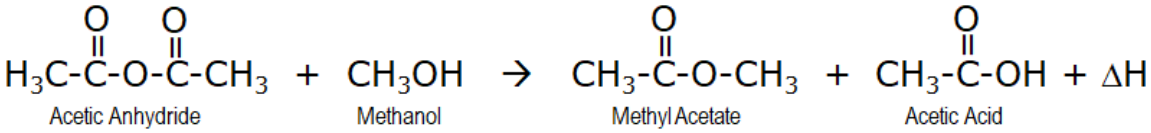


With consideration for autocatalysis:

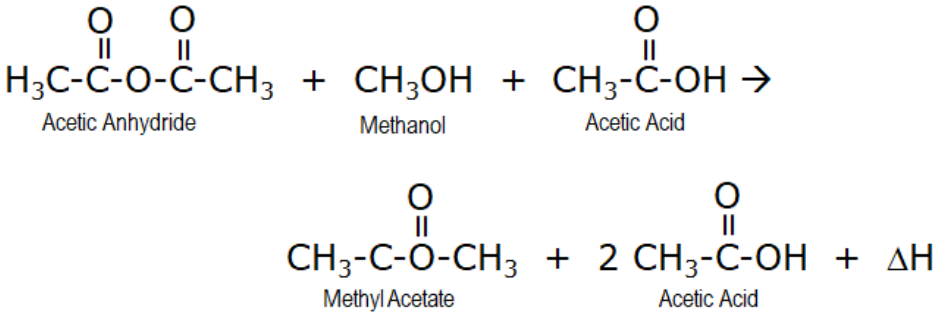


The reaction mixture of this evaluation contains excess methanol, which can react with acetic acid:

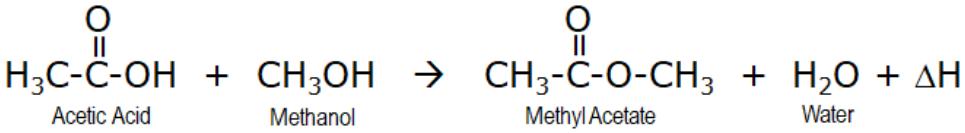


The reaction of acetic acid with methanol is much slower than the main reaction of acetic anhydride with methanol and it was not considered in the modeling. However, it is sufficient to produce hydrogen ions from acetic acid, thus providing the means for autocatalysis.

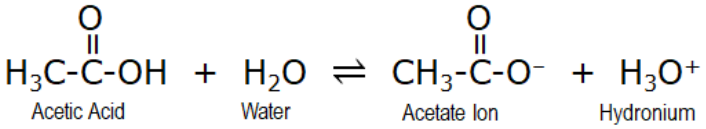

## Kinetic Development Approaches

Four kinetic approaches will be used in this development:

- Approach 1: Single reaction, no consideration for autocatalysis of acetic acid
- Approach 2: Single reaction, autocatalysis of acetic acid indirectly accounted for, by adjusting the reaction order
- Approach 3: Single reaction, autocatalysis of acetic acid
- Approach 4: Two overlapping reactions:
    - One reaction without autocatalysis
    - One reaction with autocatalysis of acetic acid

This white paper discusses the means to obtain kinetic parameters for dynamic simulations of the runaway reaction between acetic acid and methanol. The parameters are the activation energy, the pre-exponential factor, and the autocatalysis reaction order when applicable. The activation energy and pre-exponential factor can be found through different methods, such as trial and error, spreadsheet calculation, and statistical analysis, with increasing accuracy in this order.

The stoichiometry provided in this white paper is specific to the example provided.

The techniques described in this document are not intended to replace adiabatic testing. In reality, these methods need laboratory experiments to develop kinetic parameters. A single experiment sufficed for the present study and parameter variation was based entirely on SuperChems™ dynamic simulations. Kinetic development for complex conditions, involving composition variation, may require multiple runaway reaction adiabatic experiments.

## The Adiabatic Experiment and Thermal Inertia

The data from an adiabatic runaway reaction between acetic anhydride and methanol in an ARC test cell was obtained from a 1988 DIERS round-robin:

- 3.971 g of acetic anhydride
- 2.535 g of methanol
- Reaction mixture mass: 3.971+2.535 = 6.506 g

On a molar basis:

> 3.971 g/(102.0900 g/g-mol) acetic anhydride per 2.535 g/(32.0422 g/g-mol) methanol, or 0.0388971 g-mol acetic anhydride per 0.0791144 g-mol methanol

The number of moles of methanol per mole of acetic anhydride is calculated as follows:

> 1 g-mol of acetic anhydride per 0.0791144/0.0388971 g-mol of methanol, or 1 g-mol of acetic anhydride per 2.0339 g-mol of methanol

Acetic anhydride is the concentration-limiting reactant.

Test cell:

- Material of construction: Hastelloy C
- Mass: 17.829 g
- Fittings: Not provided. The fittings' mass was assumed to be 6 g, a typical value, also Hastelloy C. Arbitrarily, half the fittings mass was considered for thermal inertia calculation.

The thermal inertia of the experiment, also known as the $\phi$-factor, depends on the mass of each component and the specific heat at constant volume. After all, the test volume is practically kept constant. It is common to replace the specific heat at constant volume with the more commonly available specific heat at constant pressure. SuperChems™ calculates the specific heat of mixtures at constant volume and constant pressure at a temperature stipulated by the user. The $\phi$-factor will be somewhat different, depending on the type of specific heat.

The specific heats are the following:

- From SuperChems™, the specific heat at a constant volume for the starting mixture at the mean experimental temperature of 66.7°C is 1829 J/(kg °C).

- Test cell and fittings: Hastelloy C, specific heat 369 J/(kg °C) at the mean reaction temperature of 66.7°C. For solids, the specific heats at constant volume and constant pressure are the same, 369 J/(kg °C).

The ϕ-factor or thermal inertia of the experiment is then:

$$\phi = \frac{(6.506)(1829)+(17.829)(369)+(3)(369)}{(6.506)(1829)} = 1.65$$

## Reaction Models with and without Autocatalysis

Autocatalysis has a significant effect on the plot of self-heating rate versus temperature. Consider the Arrhenius plots of Figures 1 and 2 representing general exothermic reactions without and with autocatalysis. A reaction is autocatalytic if one of the products is a catalyst for the reaction that produced it (Approach 3) or an overlapping reaction (Approach 4).

Figure 1: Chemical reaction with no autocatalysis

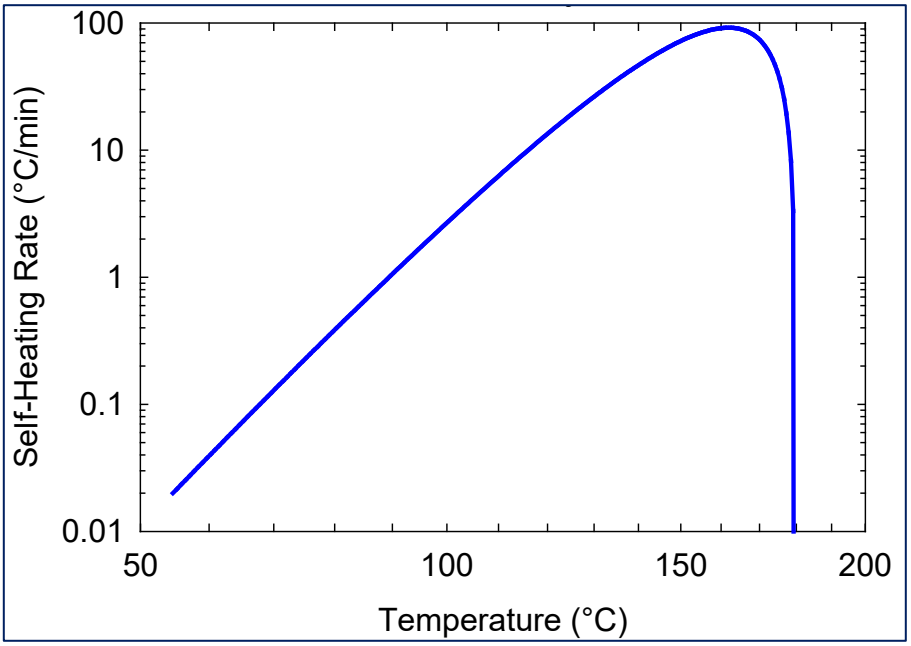

Figure 2: Chemical reaction with autocatalysis

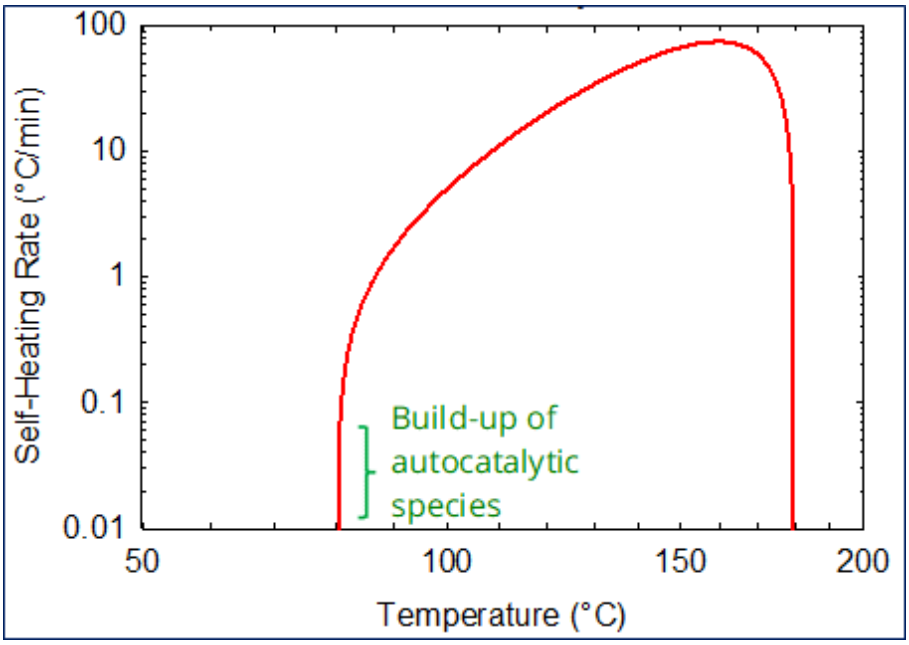


The shapes of the curves are quite different at the reaction onset: almost a straight line without autocatalysis and a visible curvature with autocatalysis. In an Arrhenius plot, an autocatalytic reaction is characterized by a slow rise in reactivity with hardly any temperature increase until there is a significant build-up of the autocatalytic species. After it happens, the runaway reaction quickly develops.

## Approach 1: Single Reaction, No Autocatalysis

This is the simplest possible approach. The rate of acetic anhydride consumption is the following:

$$-\frac{dC_a}{dt} = k' C_a^n C_m^m \qquad (1)$$

Based on conversion:

2.0339 moles of methanol per mole of acetic anhydride

$$C_a = C_{ao}(1-X);\ C_m = C_{ao}\left[1.0339 + (1-X)\right] = C_{ao}(2.0339 - X) \qquad (2)$$

$$-C_{ao}\frac{d(1-X)}{dt}=k'C_{ao}^{n}(1-X)^{n}C_{ao}^{m}(2.0339-X)^{m}$$

(3)

or

$$-\frac{d(1-X)}{dt}=k'C_{ao}^{m+n-1}(1-X)^{n}(2.0339-X)^{m}$$

(4)

$$1-X=\frac{T_f-T}{\Delta T_a};\ 2.0339-X=\frac{T_f-T+1.0339\Delta T_a}{\Delta T_a};\ T_o<T<T_f$$

(5)

$$\frac{-1}{\Delta T_a}\frac{d(T_f-T)}{dt}=kC_{ao}^{m+n-1}\left(\frac{T_f-T}{\Delta T_a}\right)^{n}\left(\frac{T_f-T+1.0339\Delta T_a}{\Delta T_a}\right)^{m}$$

(6)

$$\frac{dT}{dt}=k\left(\frac{C_{ao}}{\Delta T_a}\right)^{m+n-1}(T_f-T)^{n}(T_f-T+1.0339\Delta T_a)^{m}$$

(7)

$$\frac{dT}{dt}=k(T_f-T)^{n}(T_f-T+1.0339\Delta T_a)^{m};\ k'\left(\frac{C_{ao}}{\Delta T_a}\right)^{m+n-1}=k=k_o e^{-\frac{B}{T}}$$

(8)

$$\frac{dT}{dt} = k_o \left(T_f - T\right)^n \left(T_f - T + 1.0339\Delta T_a\right)^m e^{-\frac{B}{T}}$$

(9)

Transform Equation (9) using logarithms to yield Equation (10).

$$\ln\left(\frac{dT}{dt}\right) = \ln\left(k_o\right) + \ln\left[\left(T_f - T\right)^n \left(T_f - T + 1.0339\Delta T_a\right)^m\right] - \frac{B}{T}$$

(10)

A convenient approach to determine the activation energy is to lump all logarithmic terms of experimental data. Equation (10) is rewritten as follows:

$$\ln\left[\frac{1}{\left(T_f - T\right)^n \left(T_f - T + 1.0339\Delta T_a\right)^m}\left(\frac{dT}{dt}\right)\right] = \ln\left(k_o\right) - \frac{B}{T}$$

(11)

With this method, an Excel spreadsheet can be developed from the ARC dataset to yield an intercept [$\ln(k_o)$] and a slope (B) by straight-line regression. The most logical assumption is m = n = 1, i.e., a first-order reaction in both reactants. This will be demonstrated next. The results are the following:

- Intercept, $\ln(k_o)$: 19.43345 or $k_o = 2.7532 \times 10^8$ $(K\ min)^{-1}$
- Slope, B: 9447 K
- $R^2$: 0.9989 (coefficient of determination)

Figure 3 plots Equation (11) in an inverse Arrhenius plot. Kinetic Lumping in the y-axis is the left-hand side of Equation (11).

Figure 3: Experimental Data and Regression Based on Equation (11), m = n = 1, Reaction Order 2

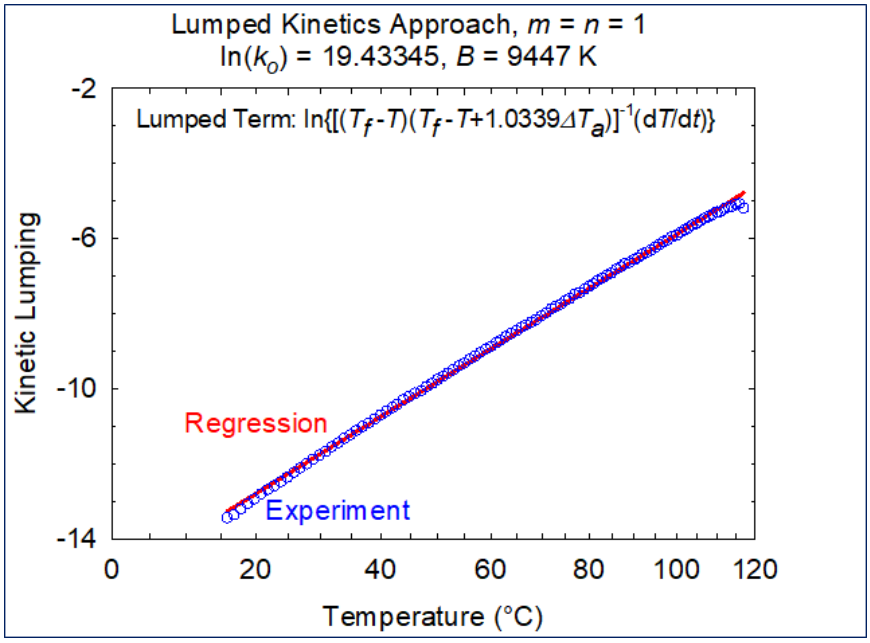


In Figure 3, the reaction order was assumed to be 2: first order in acetic anhydride and methanol. Let us consider the different orders of reaction in Figure 4. The black lines were drawn in the graph to verify linearity, i.e., they are not model-generated.

The correct order is obtained from the curve which is the closest to being linear, in which case the overall order is 2. The lines for the overall orders 1 and 3 show significant curvatures so they can be disregarded.

Figure 4: Regression with different reaction orders. Lumped kinetics approach, m = n

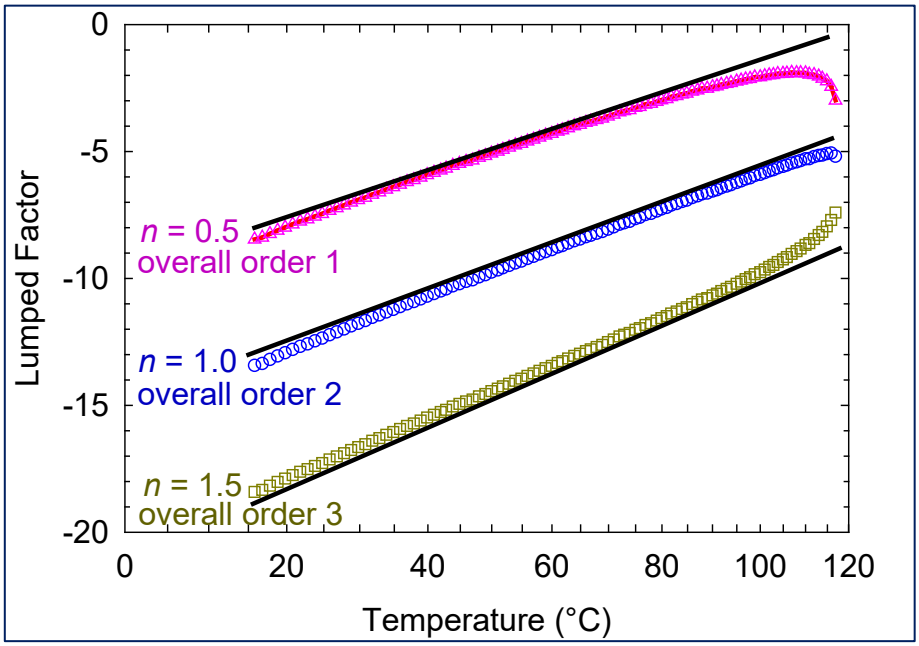


The line of overall reaction order 2 shows a slight curvature. A straight line would have been obtained with reaction order 2.2 (1.1 each for acetic anhydride and methanol). An integer reaction order of 2 makes more sense than 2.2, so order 2 was adopted for Approach 1, the simplest way to determine the pre-exponential factor. Order 2.2 is explored in Approach 2.

The pre-exponential factor based on Approaches 1 and 2, $k_o$, is unsuited for dynamic simulations, as the units are not applicable. Converting $k_o$ to appropriate units is a starting point for estimating $k_o$'.

Once the pre-exponential factor $k_o$ is determined, $k_o$' can be obtained by performing a series of trials in SuperChems™ with assumed values of $k_o$'. The estimated values of $k_o$' must be reasonably close to the actual one for this approach to be successful. In this development, the initial estimate of $k_o$' is based on $k_o$, as obtained from the straight line of the lumped kinetics.

Estimate of the pre-exponential factor for dynamic simulations starts by considering Equation (2), which results in Equation (12):

$$k' = k\left(\frac{C_{ao}}{\Delta T_a}\right)^{m+n-1} \qquad (12)$$

Then,

$$k_o' e^{-\frac{B}{T}} = k_o e^{-\frac{B}{T}} \left( \frac{\Delta T_a}{C_{ao}} \right)^{m+n-1} \tag{13}$$

or

$$k_o' = k_o \left( \frac{\Delta T_a}{C_{ao}} \right)^{m+n-1} \tag{14}$$

$k_o$, $\Delta T_a$, m, and n are known, but $C_{ao}$ must be calculated.

- $k_o = 2.7521 \times 10^8$ $(K\ min)^{-1}$
- $\Delta T_a$: See below
- m = n = 1 (first order in acetic anhydride and methanol)

Background information based on the ARC experiment:

- $T_f$ = 117.68°C, final temperature
- $T_o$ = 15.79°C, initial temperature
- T = 98.80°C, temperature at peak exotherm
- $\Delta T_a = T_f - T_a$ = 117.68 - 15.79 = 101.89°C
- dT/dt = 6.125°C/min, ARC experiment's peak exotherm at 98.80°C
- Initial mass fraction of acetic anhydride = 0.61036
- Formula weight of acetic anhydride = 102.0900
- Initial experimental pressure = 20.3 psia
- B = E/R = 9447 K
- m = n = 1
- ARC sample mass: 6.506 g = $6.506 \times 10^{-3}$ kg
- Density at initial temperature and pressure = 950.9 kg/m³ (SuperChems™ Property Estimate)
- Sample liquid volume = $6.506 \times 10^{-3}$ kg/950.9 kg/m³ = $6.8418 \times 10^{-6}$ m³
- Acetic anhydride mass = $6.506 \times 10^{-3}$ kg x 0.61036 = $3.9710 \times 10^{-3}$ kg
- Acetic anhydride moles = $3.97 \times 10^{-3}$ kg/102.0900 kg/kg-mol = $3.8897 \times 10^{-5}$ kg-mol

- $C_{ao}$ = (kg-moles of acetic anhydride)/(sample liquid volume) = 3.8897x10$^{-5}$/ 6.8418x10$^{-6}$ = 5.6851 kg-mol/m$^3$

The estimate of the pre-exponential factor for dynamic simulations is based on the background information and Equation (15), which comes from Equation (14).

$$k_o' = k_o\left(\frac{\Delta T_a}{C_{ao}}\right)^{m+n-1} = 2.7532x10^8\,\frac{1}{K\ min}\,\frac{1min}{60s}\left(\frac{101.89K}{5.6851\ \frac{kg\text{-}mol}{m^3}}\right)^{1+1-1}$$

(15)

Equation (15) results in Equation (16), which is the starting point to establish $k_o$' for dynamic simulations.

$$k_o' = 8.2240x10^7\,\frac{m^3}{kg\text{-}mol\ s}$$

(16)

The calculated $k_o$' for dynamic simulations is 9.5094x10$^7$ m$^3$/(kg-mol s), as shown next. The deviation from Equation (16) is then

$$100\frac{9.5094x10^7 - 8.2240x10^7}{9.5094x10^7} = 13.5\%$$

(17)

$k_o$' estimated by this method was in the range of the value obtained based on dynamic calculations. It is essential to apply Equation (14) to generate an estimate for $k_o$', as $k_o$ from the temperature-only modeling, Equation (11), is too far from the actual pre-exponential factor and cannot be directly used to determine $k_o$' for dynamic simulations.

The determination of the pre-exponential factor with SuperChems™ dynamic simulations involved four trials. The starting point for $k_o$' was Equation (16). The other trials assumed $k_o$' values near the starting point. The activation energy/universal gas constant value, B, was 9447 K, from a second-order reaction. The trials were such that two outputs were above, and two below the experimental self-heating rate vs. temperature curve. The experimental data and the outputs from four dynamic simulation trials are shown in Figure 5.

Figure 5: Search for the best match of the pre-exponential factor for Approach 1

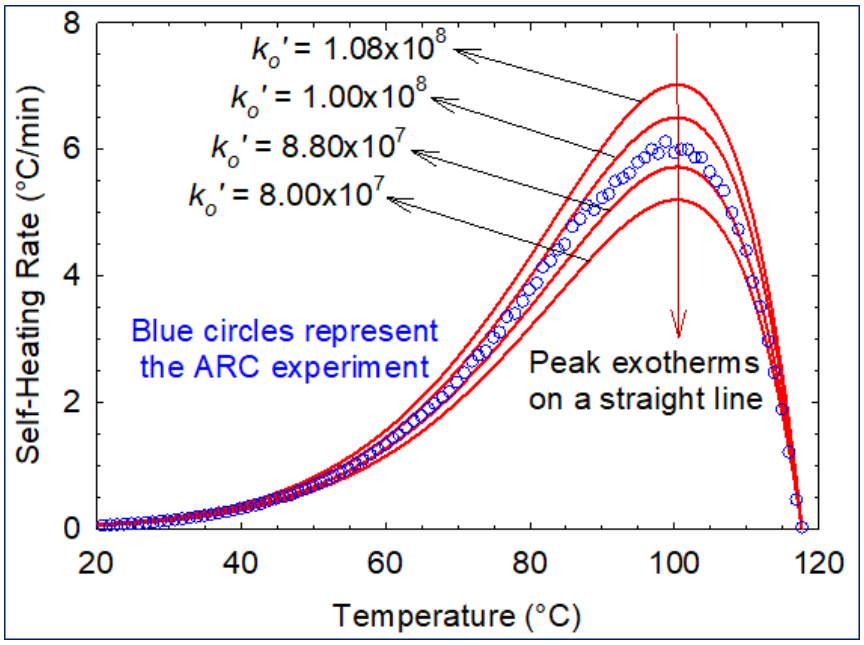


A linear scale was used in Figure 5 because the lines would be too close together on a reverse Arrhenius plot. The SuperChems™ calculated pre-exponential factors with B = 9447 K are in Table 1:

Table 1: Peak exotherms for different pre-exponential factors of Figure 5

| Pre-exponential factor [$m^3$/(kg-mol s)] | Peak exotherm (°C/min) |
|---|---|
| $8.00x10^7$ | 5.1526 |
| $8.80x10^7$ | 5.6693 |
| $1.00x10^8$ | 6.4427 |
| $1.08x10^8$ | 6.9539 |

In Figure 5 and Table 1, two values of peak exotherm are below and two are above the experimental value of 6.125°C/min. Excel Forecast can be used to obtain $k_o$' to yield 6.125°C/min for the peak exotherm. Peaks are in a straight line.

For Excel Forecast:

Known Xs: predictors, simulated peak exotherms. Assume in Excel to be cells B1 to B4.

Known Ys: responses, pre-exponential factors. Assume in Excel to be in cells A1 to A4.

Then, =FORECAST(6.125,A1:A4,B1:B4) yields $k_o$' equal to 9.5094x10$^7$ m$^3$/(kg-mol s).

dC/dt is in units of [kg-mol/(m$^3$ s)]. Therefore, for a second-order reaction, $k_o$' must have units of [m$^3$/(kg-mol s)]. There is a good match between experiment and simulation as seen in Figure 6, when the estimated value of the pre-exponential factor is entered in SuperChems™ for a dynamic simulation.

Figure 6: The best match between experimental data and simulation for Approach 1

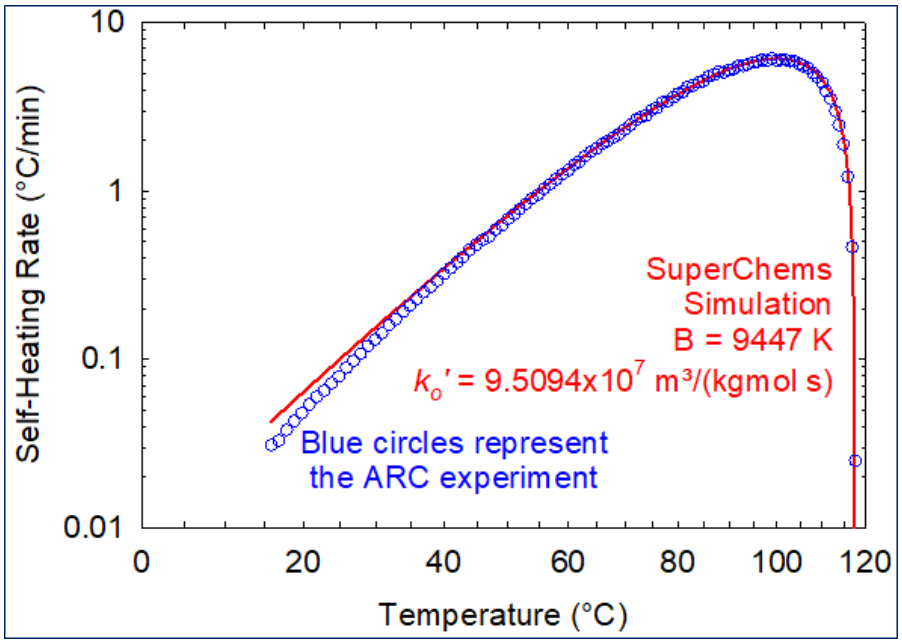


The deviation between the experiment and simulation at lower temperatures in Figure 6 is due to the assumption of reaction order 2 without autocatalysis. This reaction is mildly autocatalytic. The consequence of ignoring autocatalysis in this chemical reaction for a dynamic simulation of industrial equipment is mainly in the time to reach the pressure that opens the relief device.

To summarize, based on the development of Approach 1, the kinetic parameters for dynamic simulations are $k_o$' = 9.5094x10$^7$ m$^3$/(kg-mol s) and B = 9447 K.

## Approach 2: Single Reaction, Autocatalysis

If in Figure 4 the curve for n = 1 (overall order 2) is replaced with another curve with n = 2.2 (overall order 2.2), the following is obtained in Figure 7:

Figure 7: Regression with different reaction orders. Lumped kinetics approach, m = n

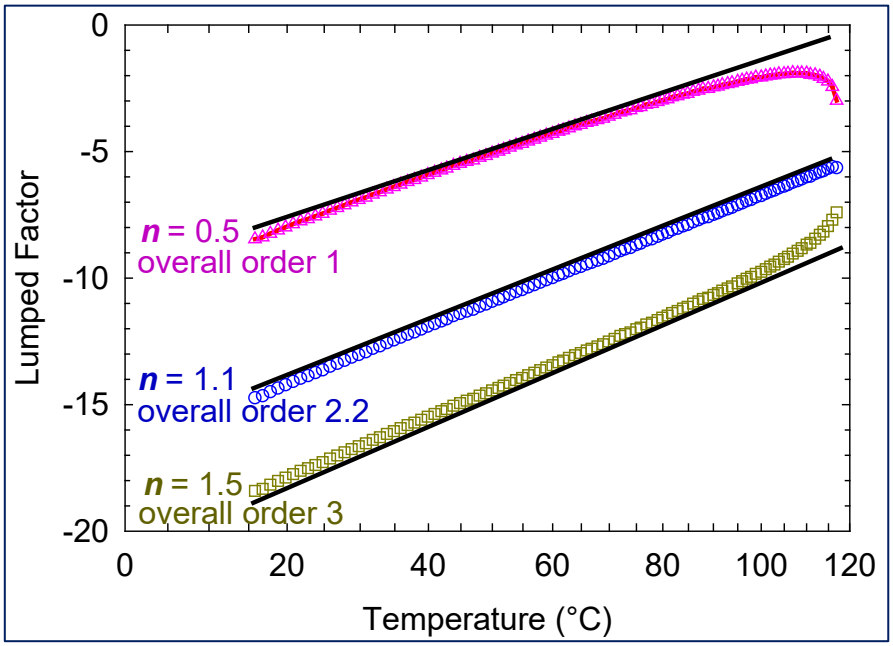


Comparing Figures 4 and 7, it can be seen that n = 1.1 yields a straighter line than n = 1. Figure 8 can be obtained through Equation (11).

Figure 8: Lumped kinetic approach for n = 1.1. $\ln(k_o)$ = 20.5069, B = 10153 K

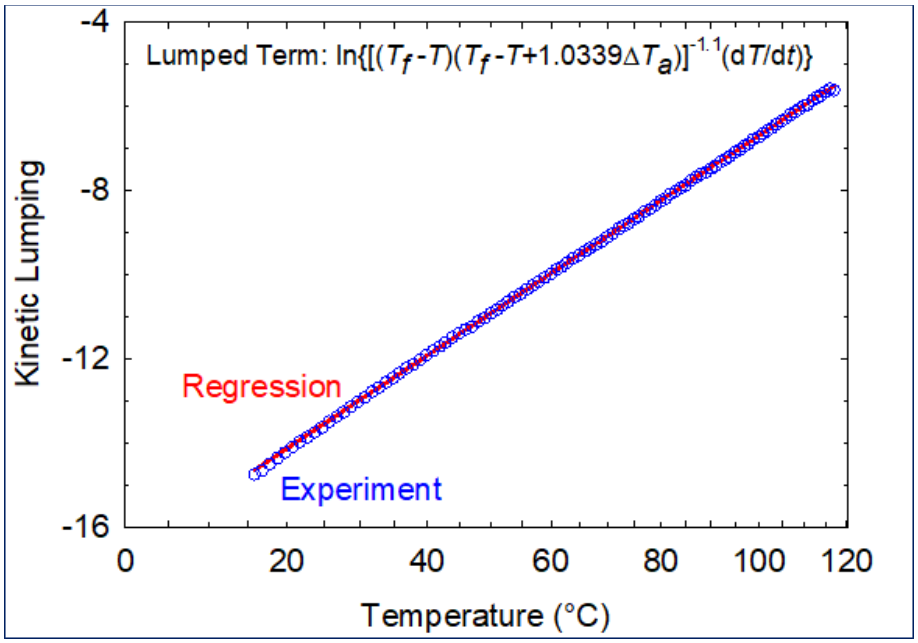

$k_o$' can be developed starting with $k_o = \exp(20.5069) = 8.0544x10^8$ with $C_{ao}$ developed in Approach 1. From Equation (8),

$$k_o' = k_o\left(\frac{\Delta T_a}{C_{ao}}\right)^{m+n-1} = 8.0544x10^8\,\frac{1}{K\ min}\,\frac{1min}{60s}\left(\frac{101.89K}{5.6851\ \frac{kgmol}{m^3}}\right)^{1.1+1.1-1} \quad (18)$$

or

$$k_o' = 4.2459x10^8\left(\frac{m^3}{kgmol}\right)^{1.2}\frac{K^{0.2}}{s} \quad (19)$$

The same Approach 1 procedure applies to Approach 2. Two points above and two below $k_o$' are chosen for dynamic simulations. Then, Excel Forecast is applied to the resulting pairs of self-heating rates dT/dt and pre-exponential factors $k_o$' to yield the outcome in Equation (20).

$$k_o' = 5.3500x10^8\left(\frac{m^3}{kgmol}\right)^{1.2}\frac{K^{0.2}}{s} \quad (20)$$

The inverse Arrhenius plot of self-heating rate vs. temperature for Approach 2 can be visualized in Figure 9.

Figure 9: The best match between experimental data and simulation for Approach 2

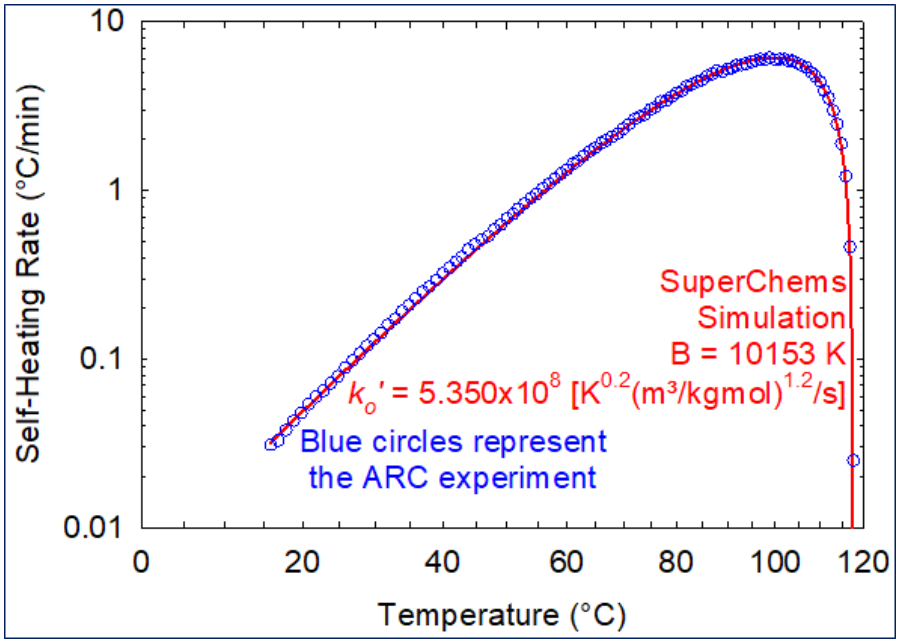

The kinetic match with m = n = 1.1 is superior to m = n = 1. This is a mathematical artifact representing the autocatalytic effect of acetic anhydride, as explained next.

Reactions of water or alcohol with anhydrides are acid-catalyzed. Acetic acid is a weak acid formed in this chemical reaction. Hence, a modest autocatalytic effect might be responsible for the extra 0.2 in the reaction order. This effect is observed in the ARC adiabatic experiment's self-heating data at lower temperatures but is more obvious in isothermal data.

Other known reactions occur to a small degree under these conditions. For example, acetic acid dimerizes, which might reduce its effectiveness as a catalyst, and its consequence is accounted for in the data. A truly autocatalytic model may fit the data better, examined in Approaches 3 and 4.

## Approach 3: Single Reaction, Autocatalysis of Acetic Acid

With autocatalysis by acetic acid, the rate of acetic anhydride consumption can be expressed by Equation (21).

$$-\frac{dC_a}{dt} = kC_a^n C_m^m C_c^j \quad (21)$$

Comparing Equations (1) and (21), the latter is augmented by the acetic acid concentration raised to a certain order j. There is no need for an acetic acid seed in the initial mixture. The SuperChems™ dynamic simulation leads to autocatalysis even with the initial acetic acid concentration set to zero.

As in Approaches 1 and 2, the concentrations in Equation (21) can be expressed as conversions:

$$C_a = C_{ao}(1-X);\ C_m = C_{ao}\left[1.0339+(1-X)\right] = C_{ao}(2.0339-X); C_j = C_{ao}X \quad (22)$$

The reaction rate of acetic anhydride, the limiting species, can be expressed as follows:

$$-C_{ao}\frac{d(1-X)}{dt} = kC_{ao}^n(1-X)^n C_{ao}^m(2.0339-X)^m C_{ao}^j X \quad (23)$$

or

$$-\frac{d(1-X)}{dt} = kC_{ao}^{m+n+j-1}(1-X)^n(2.0339-X)^m X^j \quad (24)$$

The reactant conversion can be expressed as temperature:

$$1-X=\frac{T_f-T}{\Delta T_a};\ 2.0339-X=\frac{T_f-T+1.0339\Delta T_a}{\Delta T_a};\ X=\frac{T-T_o}{\Delta T_a};\ T_o<T<T_f \tag{25}$$

Then,

$$\frac{-1}{\Delta T_a}\frac{d\left(T_f-T\right)}{dt}=kC_{ao}^{m+n+j-1}\left(\frac{T_f-T}{\Delta T_a}\right)^n\left(\frac{T_f-T+1.0339\Delta T_a}{\Delta T_a}\right)^m\left(\frac{T-T_o}{\Delta T_a}\right)^j \tag{26}$$

or

$$\frac{dT}{dt}=k\left(\frac{C_{ao}}{\Delta T_a}\right)^{m+n+j-1}\left(T_f-T\right)^n\left(T_f-T+1.0339\Delta T_a\right)^m\left(T-T_o\right)^j \tag{27}$$

or

$$\frac{dT}{dt}=k'\left(T_f-T\right)^n\left(T_f-T+1.0339\Delta T_a\right)^m\left(T-T_o\right)^j;\ k\left(\frac{C_{ao}}{\Delta T_a}\right)^{m+n+j-1}=k'=k_o'e^{-\frac{B}{T}} \tag{28}$$

or

$$\frac{dT}{dt}=k_o'\left(T_f-T\right)^n\left(T_f-T+1.0339\Delta T_a\right)^m\left(T-T_o\right)^j e^{-\frac{B}{T}} \tag{29}$$

Equation (29) can be transformed with logarithms to yield Equation (30):

$$\mathrm{n}\left(\frac{dT}{dt}\right)=\ln\left(k_o'\right)+\ln\left[\left(T_f-T\right)^n\left(T_f-T+1.0339\Delta T_a\right)^m\left(T-T_o\right)^j\right]-\frac{B}{T} \tag{30}$$

A convenient approach to determine the activation energy is to lump all logarithmic terms of experimental data. Equation (30) is rewritten as follows:

$$\ln\left[\frac{1}{\left(T_f-T\right)^n\left(T_f-T+1.0339\Delta T_a\right)^m\left(T-T_o\right)^j}\left(\frac{dT}{dt}\right)\right]=\ln\left(k_o'\right)-\frac{B}{T} \tag{31}$$

With this method, an Excel spreadsheet can be developed from the ARC dataset to yield an intercept [ln($k_o$')] and a slope (B). The real intent is to obtain j in Equation (31). The most logical assumption is m = n = 1, i.e., a first-order reaction in acetic anhydride and methanol as in Approach 1. The value of j can be varied to obtain the best possible straight line.

The first step is to assume j = 0. As such, the results of Approach 1 are reproduced. The second step is to vary j to optimize the linearity through the Pearson correlation coefficient (R), which measures the degree of linearity between two variables.

The Pearson Correlation Coefficient varies between -1 and +1. The closer the coefficient is to these two extremes, the higher the linear relationship. When one variable decreases while the other increases, the coefficient is negative. When both variables change in the same direction, the coefficient is positive. The linearity is the highest when R is 1 for positive or -1 for negative correlation.

The Pearson Correlation Coefficient (R) is calculated as follows:

$$R = \frac{\sum_{i=1}^{n}\left(x_i - \bar{x}\right)\left(y_i - \bar{y}\right)}{\left(n-1\right)s_x s_y} \tag{32}$$

where

$x_i$ = point of the first variable, inverse temperature on an absolute scale

$y_i$ = point of the second variable, left-hand side of Equation (31)

$\bar{x}$ = sample mean for the first variable

$\bar{y}$ = sample mean for the second variable

n = column length

$s_x$ = standard deviation for the first variable

$s_y$ = standard deviation for the second variable

The linearity analysis is presented in Figure 10 for variable autocatalysis exponent j

Figure 10: Optimization of autocatalysis coefficient with Pearson Correlation Coefficient

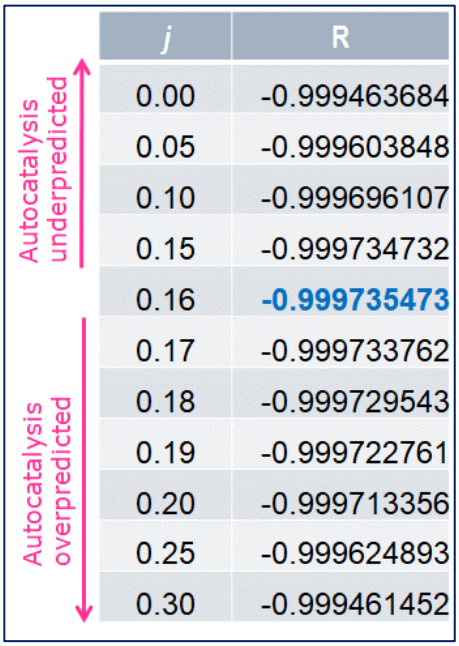


| j | R |
|---|---|
| 0.00 | -0.999463684 |
| 0.05 | -0.999603848 |
| 0.10 | -0.999696107 |
| 0.15 | -0.999734732 |
| 0.16 | **-0.999735473** |
| 0.17 | -0.999733762 |
| 0.18 | -0.999729543 |
| 0.19 | -0.999722761 |
| 0.20 | -0.999713356 |
| 0.25 | -0.999624893 |
| 0.30 | -0.999461452 |

As seen in Figure 10, the correlation between inverse temperature and the left-hand side of Equation (31) is negative. The highest value of the Pearson Correlation Coefficient on the negative side is for j equal to 0.16.

By following the procedure of Approaches 1 and 2, the following kinetic parameters are obtained:

Intercept, $\ln(k_o) = 17.23875$, from which $k_o = 30668574$ K min$^{-1}$

Slope, B: 8903 K

$$k_o' = k_o\left(\frac{\Delta T_a}{C_{ao}}\right)^{m+n-1} = 30668574\,\frac{1}{K\ min}\,\frac{1min}{60\,s}\left(\frac{101.89\,K}{5.6851\ \frac{kg\text{-}mol}{m^3}}\right)^{1+1+0.16-1} \tag{33}$$

$$= 1.4531x10^7\left(\frac{m^3}{kg\text{-}mol}\right)^{1.16}\frac{K^{0.16}}{s}$$

The two terms are in red because the Pearson Correlation Coefficient method is inadequate to establish parameters for dynamic simulations. The approach is useful to estimate the reaction order j, but B and $k_o$' are flawed. More advanced statistics can provide the means to identify

these parameters. Note that the autocatalytic coefficient j could also be part of the design. This is shown in Approach 4.

The goal of statistics optimization is to match the outputs, which are experimental self-heating rates at two conveniently chosen temperatures:

- At the low end, 30°C: 0.1351°C/min
- At the peak exotherm: 6.1250°C/min

These two values are the responses for the Response Surface Methodology (RSM) with Central Composite Design (CCD). Dynamic simulations must produce values close to these targets with the optimization procedure. The intent of this white paper is not to teach statistics. There are publications that the reader might consult, such as Box [3], Kiemele et al. [4], Montgomery [5], and Spiegel and Stephens [6].

Model parameters in statistics are called predictors, in this case, B and $k_o$'. Knowledge of experimental design in statistics is advantageous to understand the solutions to Approaches 3 and 4.

The Central Composite Design for Approach 3 was modified with one central point instead of the standard model with five central points for two predictors. The reason is that the "experiments" in this evaluation are dynamic simulations with SuperChems™. The results are identical with any number of runs for the same values of the predictors. Minitab is the statistical software used in this development (Approaches 3 and 4). Other advanced statistical software could also be used.

Many predictors can be included in the design, such as pre-exponential factors, activation energies, reaction orders, binary interaction parameters, and so forth. However, the design becomes increasingly complex as the number of predictors increases. For CCD with one central point, the number of SuperChems™ simulations is $2^k+2k+1$, where k is the number of predictors. For two predictors, $2^2+2x2+1 = 9$ simulations are needed for the initial design. The number of simulations escalates to 15 for three predictors and 25 for four predictors. Hence, there is a practical interest in keeping the number of predictors as low as possible and using other means to establish some parameters. This is why the Pearson Correlation Coefficient was used to determine j.

The parameters established with the Pearson Correlation Coefficient are not accurate for dynamic simulations, but they provide a certain order of magnitude to identify the optimum parameters. The parameter B of the activation energy was estimated at 8903 K, so the experimental design must include values of B in a range that does not necessarily include that

value but should be close. The range chosen was 9150 to 9300 K. The parameter $k_o$' was estimated at 1.4531x10$^7$ with units shown in Equation (33). The range chosen was 4x10$^7$ to 5x10$^7$. These B and $k_o$' ranges were not set arbitrarily. A few SuperChems™ runs were made to establish the design range, as shown in Figure 11.

Figure 11: Response Surface with Central Composite Design for Approach 3

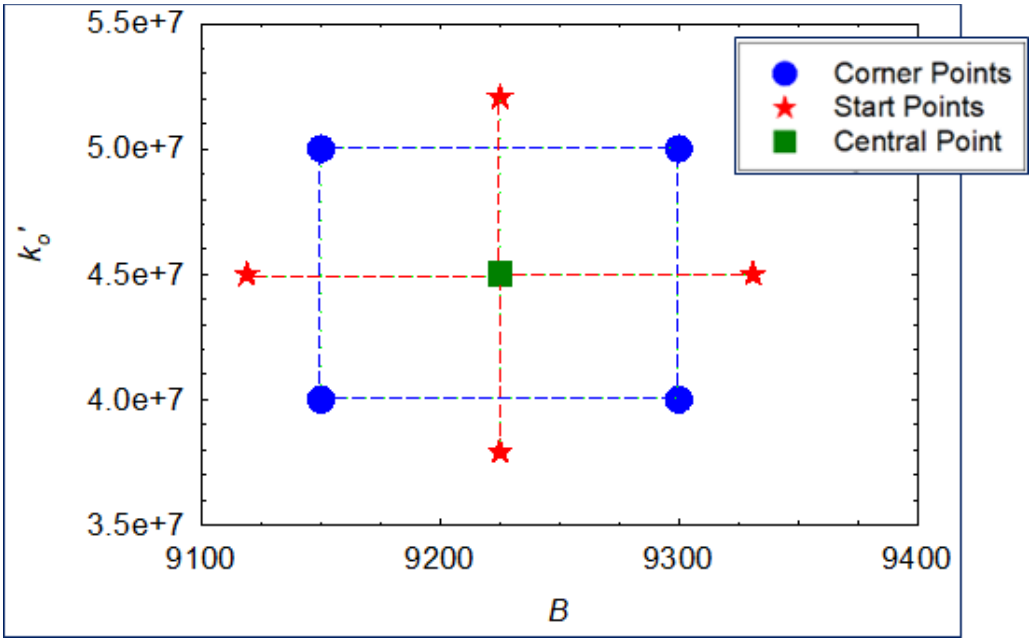


The simulation results are in Table 2.

Table 2: Simulations for the first design of Approach 3

| Run | B | $k_o$' | T' at 30°C | T' max | Type |
|---|---|---|---|---|---|
| 1 | 9300 | 5.00E+07 | 0.1281 | 5.9997 | CP |
| 2 | 9225 | 4.50E+07 | 0.1472 | 6.6012 | CtrP |
| 3 | 9150 | 4.00E+07 | 0.1679 | 7.1738 | CP |
| 4 | 9331.07 | 4.50E+07 | 0.1048 | 4.9673 | SP |
| 5 | 9118.93 | 4.50E+07 | 0.2104 | 8.7691 | SP |
| 6 | 9300 | 4.00E+07 | 0.1025 | 4.7983 | CP |
| 7 | 9225 | 52071068 | 0.1714 | 7.6367 | SP |
| 8 | 9225 | 37928932 | 0.1246 | 5.5609 | SP |
| 9 | 9150 | 50000000 | 0.2107 | 8.9625 | CP |

Predictors Responses

T' is the self-heating rate in °C/min. The design points are CP for the corner points, SP for the star points, and CtrP for the center point.

The following terms are considered to optimize the model for the given responses, the self-heating rates at 30°C and the peak:

- Intercept
- Linear terms: B and $k_o$'
- Square terms: B * B and $k_o$' * $k_o$'
- Interaction term: B * $k_o$'

Only $k_o$' * $k_o$' was found not to be statistically significant. Some terms in statistics need to be defined. They are the following:

- Coefficients: Estimates that multiply the predictors to estimate the fitted values of the responses.
- Standard Error of the Coefficients: Standard deviation of the error of a given predictor to estimate the responses.
- t: The value of the student t-distribution to determine the p-value (probability that the null hypothesis is true)
- p: Null-hypothesis test, whether the predictor correlates with the response. The null hypothesis (no correlation) is typically rejected at $p < 0.05$. A design of experiments can sometimes be more lenient, with the null hypothesis rejected for $p < 0.1$.
- F: The value of the F-distribution to determine the p-value in the lack-of-fit test of Analysis of Variance. It checks if an adequate model has been chosen. Model adequacy is established for $p < 0.05$ in this white paper.

Initially, the analysis is performed for each of the two responses, the self-heating rate at 30°C and the maximum. Then, the software reconciles the parameters of the two responses, B and $k_o$', into a single value for the predictors.

The statistical analysis for each response is shown in Table 3, with the $k_o$' * $k_o$' quadratic term already eliminated from the design.

Table 3: Statistical analysis for each response of the first design of Approach 3

**Estimated Regression Coefficients for ROR 30C**

| Term | Coef | SE Coef | T | P |
|---|---|---|---|---|
| Constant | 0.147600 | 0.000326 | 452.873 | 0.000 |
| B | -0.052563 | 0.000312 | -168.447 | 0.000 |
| ko | 0.023792 | 0.000312 | 76.244 | 0.000 |
| B*B | 0.009800 | 0.000565 | 17.360 | 0.000 |
| B*ko' | -0.008600 | 0.000624 | -13.780 | 0.000 |

S = 0.0006241 R-Sq = 100.0% R-Sq(adj) = 100.0%

**Analysis of Variance for ROR 30C**

| Source | DF | Seq SS | Adj SS | Adj MS | F | P |
|---|---|---|---|---|---|---|
| Regression | 4 | 0.013507 | 0.013507 | 0.003377 | 8669.75 | 0.000 |
| Linear | 2 | 0.013316 | 0.013316 | 0.006658 | 17093.86 | 0.000 |
| Square | 1 | 0.000117 | 0.000117 | 0.000117 | 301.38 | 0.000 |
| Interaction | 1 | 0.000074 | 0.000074 | 0.000074 | 189.89 | 0.000 |
| Residual Error | 4 | 0.000002 | 0.000002 | 0.000000 | | |
| Total | 8 | 0.013509 | | | | |

**Estimated Regression Coefficients for ROR Max**

| Term | Coef | SE Coef | T | P |
|---|---|---|---|---|
| Constant | 6.5995 | 0.006168 | 1069.968 | 0.000 |
| B | -1.8941 | 0.005905 | -320.750 | 0.000 |
| ko | 1.0475 | 0.005905 | 177.387 | 0.000 |
| B*B | 0.2685 | 0.010683 | 25.137 | 0.000 |
| B*ko' | -0.2936 | 0.011811 | -24.863 | 0.000 |

S = 0.01181 R-Sq = 100.0% R-Sq(adj) = 100.0%

**Analysis of Variance for ROR Max**

| Source | DF | Seq SS | Adj SS | Adj MS | F | P |
|---|---|---|---|---|---|---|
| Regression | 4 | 18.9147 | 18.9147 | 4.72867 | 33899.15 | 0.000 |
| Linear | 2 | 18.7403 | 18.7403 | 9.37015 | 67173.29 | 0.000 |
| Square | 1 | 0.0881 | 0.0881 | 0.08814 | 631.86 | 0.000 |
| Interaction | 1 | 0.0862 | 0.0862 | 0.08623 | 618.17 | 0.000 |
| Residual Error | 4 | 0.0006 | 0.0006 | 0.00014 | | |
| Total | 8 | 18.9152 | | | | |

ROR 30C: Temperature rate of rise at 30°C

ROR Max: Temperature rate of rise at the peak exotherm

The development of a single set of parameters involves an optimization procedure. In experimental design, it is done through the desirability function [7]. The higher the desirability, the better the outcome for parameter determination. The combined analysis is displayed in Figure 11.

Figure 11: First design optimization for the predictors of Approach 3

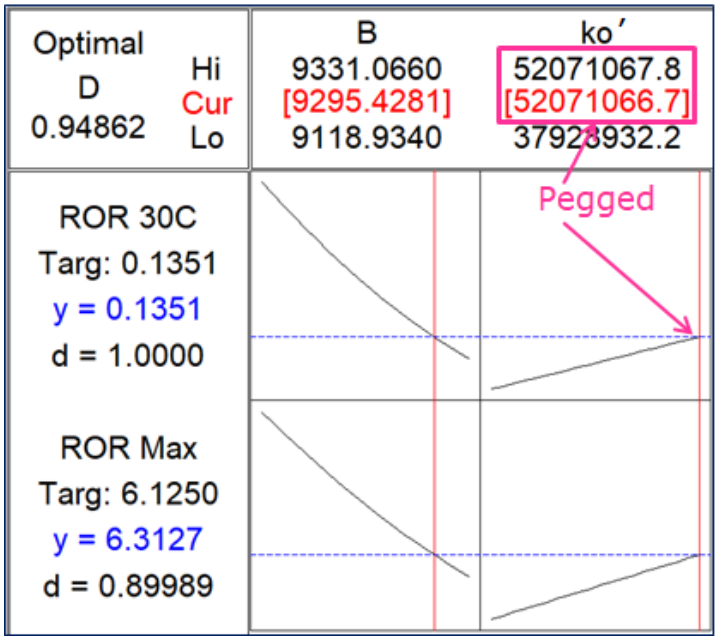

The optimal desirability D is the geometric mean of the individual desirability values d:

$$D = \sqrt[2]{d_1 d_2}$$
$$D = \sqrt[2]{(1.00000)(0.89989)}$$
$$D = 0.94862$$

Figure 11 indicates that the self-heating rate at 30°C matched very well, given the maximum desirability of 1, but the maximum self-heating rate did not, with a desirability of about 0.9. The individual optima are in red. Note that $k_o$' is pegged at the high end of the confidence interval. This is an undesirable outcome. Although the composite desirability D is quite good, a predictor's pegged value means the optimum has not been reached. A model extension with different predictor values would be needed to bring $k_o$' within the high-low range of the confidence interval.

Figure 11 indicates that $k_o$' was underpredicted because the values selected for the design were not sufficiently high to reach the optimum. An extra point was added to the design, as shown in Figure 12. Figure 12 also displays the optimum location after completing the statistical analysis. The range of the second design is adequate.

Figure 12: Response Surface with Central Composite Design for the second design of Approach 3 with an additional point

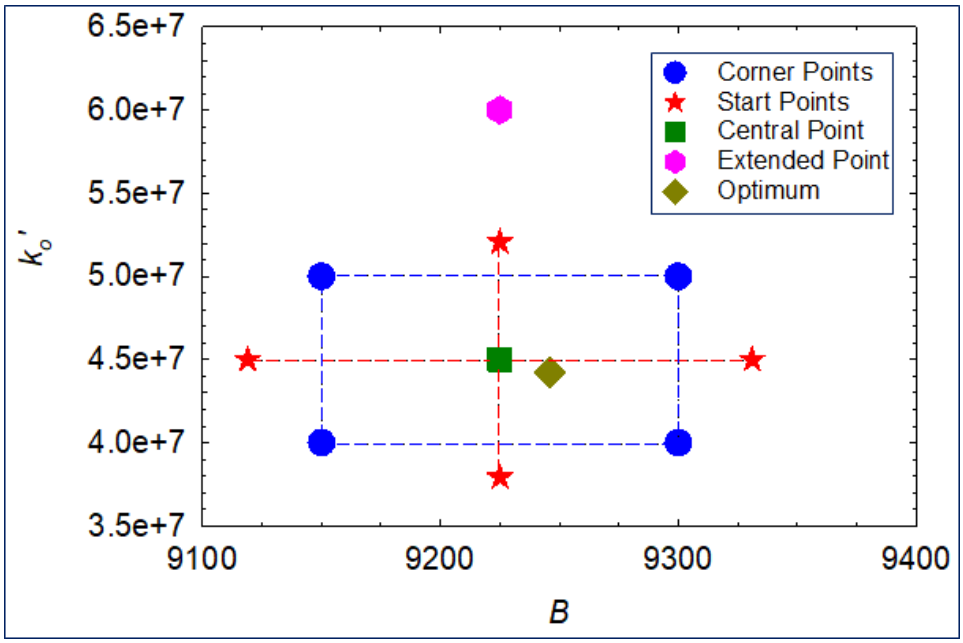

Figure 12 is quite peculiar because the optimum was within the $k_o$' range initially chosen. The extra point redefined the regression so no parameter was pegged at one end of the design range. This result is common in RSM. The points of the design are insufficient for adequate regression and adding more points can be helpful.

The simulation results with the augmented design are in Table 4. The extra point is in blue.

Table 4: Simulations for the second design of Approach 3

| Run | B | $k_o$' | T' at 30°C | T' max | Type |
|---|---|---|---|---|---|
| 1 | 9300 | 5.00E+07 | 0.1281 | 5.9997 | CP |
| 2 | 9225 | 4.50E+07 | 0.1472 | 6.6012 | CtrP |
| 3 | 9150 | 4.00E+07 | 0.1679 | 7.1738 | CP |
| 4 | 9331.07 | 4.50E+07 | 0.1048 | 4.9673 | SP |
| 5 | 9118.93 | 4.50E+07 | 0.2104 | 8.7691 | SP |
| 6 | 9300 | 4.00E+07 | 0.1025 | 4.7983 | CP |
| 7 | 9225 | 52071068 | 0.1714 | 7.6367 | SP |
| 8 | 9225 | 37928932 | 0.1246 | 5.5609 | SP |
| 9 | 9150 | 50000000 | 0.2107 | 8.9625 | CP |
| 10 | 9225 | 6.00E+07 | 0.1970 | 8.7980 | EP |

Predictors Responses

T' is the self-heating rate in °C/min. The design points are CP for the corner points, SP for the star points, CtrP for the center point, and EP for the extended point. The statistical analysis of the data in Table 4 is presented in Table 5.

Table 5: Statistical analysis for each response of the second design of Approach 3

**Estimated Regression Coefficients for ROR 30C**

| Term | Coef | SE Coef | T | P |
|---|---|---|---|---|
| Constant | 0.147600 | 0.000326 | 452.873 | 0.000 |
| B | -0.052563 | 0.000312 | -168.447 | 0.000 |
| ko | 0.023792 | 0.000312 | 76.244 | 0.000 |
| B*B | 0.009800 | 0.000565 | 17.360 | 0.000 |
| B*ko' | -0.008600 | 0.000624 | -13.780 | 0.000 |

S = 0.0006241 R-Sq = 100.0% R-Sq(adj) = 100.0%

**Analysis of Variance for ROR 30C**

| Source | DF | Seq SS | Adj SS | Adj MS | F | P |
|---|---|---|---|---|---|---|
| Regression | 4 | 0.013507 | 0.013507 | 0.003377 | 8669.75 | 0.000 |
| Linear | 2 | 0.013316 | 0.013316 | 0.006658 | 17093.86 | 0.000 |
| Square | 1 | 0.000117 | 0.000117 | 0.000117 | 301.38 | 0.000 |
| Interaction | 1 | 0.000074 | 0.000074 | 0.000074 | 189.89 | 0.000 |
| Residual Error | 4 | 0.000002 | 0.000002 | 0.000000 | | |
| Total | 8 | 0.013509 | | | | |

**Estimated Regression Coefficients for ROR Max**

| Term | Coef | SE Coef | T | P |
|---|---|---|---|---|
| Constant | 6.5995 | 0.006168 | 1069.968 | 0.000 |
| B | -1.8941 | 0.005905 | -320.750 | 0.000 |
| ko | 1.0475 | 0.005905 | 177.387 | 0.000 |
| B*B | 0.2685 | 0.010683 | 25.137 | 0.000 |
| B*ko' | -0.2936 | 0.011811 | -24.863 | 0.000 |

S = 0.01181 R-Sq = 100.0% R-Sq(adj) = 100.0%

**Analysis of Variance for ROR Max**

| Source | DF | Seq SS | Adj SS | Adj MS | F | P |
|---|---|---|---|---|---|---|
| Regression | 4 | 18.9147 | 18.9147 | 4.72867 | 33899.15 | 0.000 |
| Linear | 2 | 18.7403 | 18.7403 | 9.37015 | 67173.29 | 0.000 |
| Square | 1 | 0.0881 | 0.0881 | 0.08814 | 631.86 | 0.000 |
| Interaction | 1 | 0.0862 | 0.0862 | 0.08623 | 618.17 | 0.000 |
| Residual Error | 4 | 0.0006 | 0.0006 | 0.00014 | | |
| Total | 8 | 18.9152 | | | | |

ROR 30C: Temperature rate of rise at 30°C

ROR Max: Temperature rate of rise at the peak exotherm

Table 3 and 5 show the same statistically significant terms in the first and second designs. The desirability analysis of the second design is displayed in Figure 14.

Figure 14: Second design optimization for the predictors of Approach 3

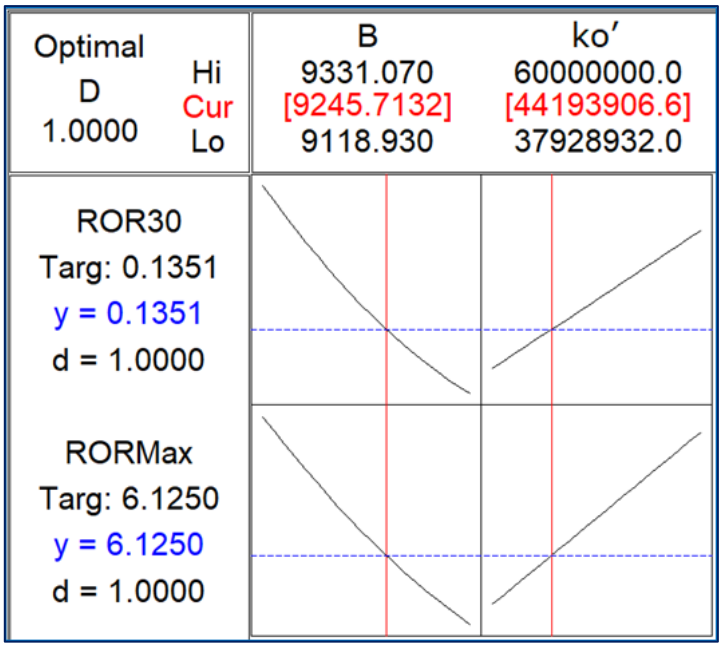

The individual optima are in red. B and $k_o$' are well within the high and low limits of the range. $k_o$' is not pegged at the high end of the confidence interval as seen in the first design in Figure 11. The individual desirability values for the self-heating rate at 30°C and the maximum self-heating rate are equal to 1, so the composite desirability is also 1.

Figure 15 shows an overlaid contour plot for the two predictors ($k_o$' and B) and a white zone, the intersection of the two response curves (self-heating rates at 30°C and the maximum) for their assigned ranges. The optimum of the design is within the white zone, as required.

Figure 15: Overlaid contour plot for the second design of Approach 3

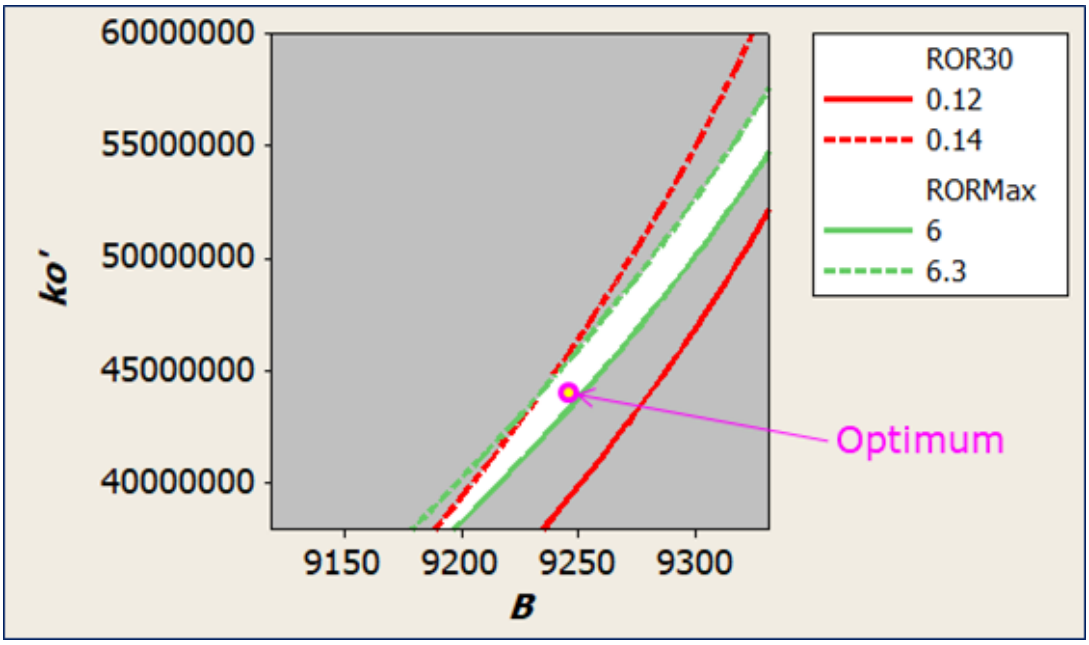


From the desirability plot, the following optimized values are obtained for the predictors:

$$B = 9246K$$

$$k_o' = 4.4194x10^7 \left(\frac{m^3}{kg\text{-}mol}\right)^{1.16} \frac{K^{0.16}}{s}$$

Figure 16 shows a reverse Arrhenius plot of the experimental data and simulation with the optimized parameters of Approach 3.

Figure 16: Comparison of the Approach 3 model with experimental data on a reverse Arrhenius scale

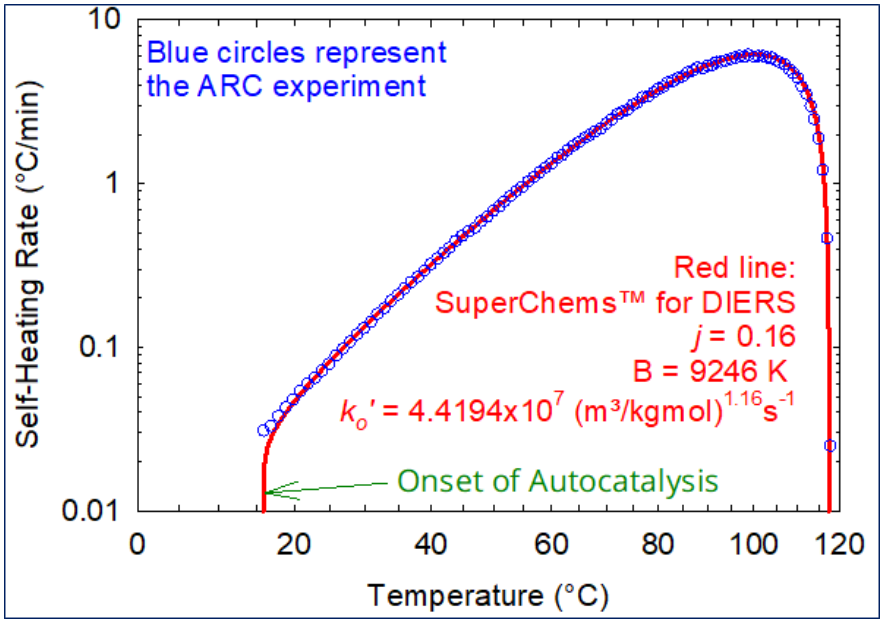


The steep rise in the simulated self-heating rate at the onset of the exotherm is characteristic of autocatalysis. See Figure 2. The ARC experiment did not register the sudden self-heating rate of rise due to the instrument's limited detection below 0.02°C/min. Figure 17 exhibits the same data in a plot with linear coordinates. The match is good on both scales.

Figure 17: Comparison of the Approach 3 model with experimental data on a linear scale

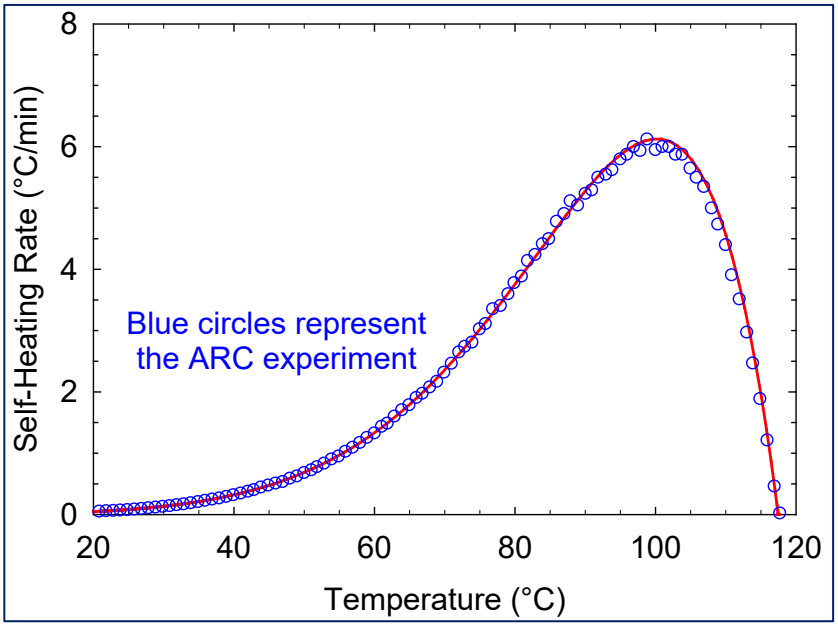

## Approach 4: Two Reactions, with and without Autocatalysis of Acetic Acid

The reactions of this model are the following [8]:

$$\text{Reaction 1: } -\frac{dC_a}{dt} = k'_{o1} e^{\frac{B_1}{T}} C_a^{n_1} C_m^{m_1} \tag{34}$$

$$\text{Reaction 2: } -\frac{dC_a}{dt} = k'_{o2} e^{\frac{B_2}{T}} C_a^{n_2} C_m^{m_2} C_c^{j} \tag{35}$$

According to this model, Reaction 1 is not autocatalytic, and Reaction 2 is autocatalytic. Assuming $m_1 = n_1 = m_2 = n_2 = 1$ as in prior approaches, and known activation energies from Bohm et al. [8], the system of Approach 4 has three parameters to be determined, according to the highlighted terms in blue in Equations (34) and (35): the pre-exponential factors $k_{o1}$' and $k_{o2}$', and the autocatalytic exponent j.

The kinetic parameters in Bohm et al. [8] are based on the molar ratio $X_o$ of acetic anhydride and methanol:

$$X_o = \frac{\text{[moles of acetic anhydride]}}{\text{[moles of acetic anhdride] + [moles of methanol]}} = \frac{1}{1+2} = \frac{1}{3} \tag{36}$$

The pre-exponential factors and activation energies were calculated as follows [8]:

$$k'_{o1} = 1.36x10^8 \left(e^{2.2X_o} - 1\right) = 1.36x10^8 \left(e^{2.2\frac{1}{3}} - 1\right) = 1.4715x10^8 \text{ [kg-mol/(m³ s)]}^{-1} \tag{37}$$

$$B_1 = 1915.2\left(X_o^2\right) + 2473.8\left(X_o\right) + 9301.5 = 10339\,K \tag{38}$$

$$k'_{o2} = 2x10^7 e^{(-12.28X_o)} = 2x10^7 e^{\left(-12.28\frac{1}{3}\right)} = 3.3367x10^5 \text{ [kg-mol/(m³ s)]}^{-(1+j)} \tag{39}$$

$$B_2 = -4867.7\left(X_o\right) + 9712.0 = 8089\,K \tag{40}$$

$k_{o1}$'and $k_{o2}$' in Equations (37) and (39) are in appropriate units for the kinetic orders.

Formulas are for activation energies $E_1$ and $E_2$ in Bohm et al. [8]. This work divides them by the universal gas constant to yield $B_1$ and $B_2$ in Equations (38) and (40). That publication also considered j = 1 for the acetic acid exponent in Equation (35).

A simulation was carried out in SuperChems™ with the kinetic parameters of Equations (37) to (40) plus j =1. The results are in Figure 18 and 19, which show a big discrepancy between experimentation and simulation. It does not mean the parameters are incorrect. Be careful when using published data! The conditions in the modeling may differ from those in the publication.

Figure 18: Inverse Arrhenius plot, experimental data and simulation with Bohms et al. [8] kinetic parameters

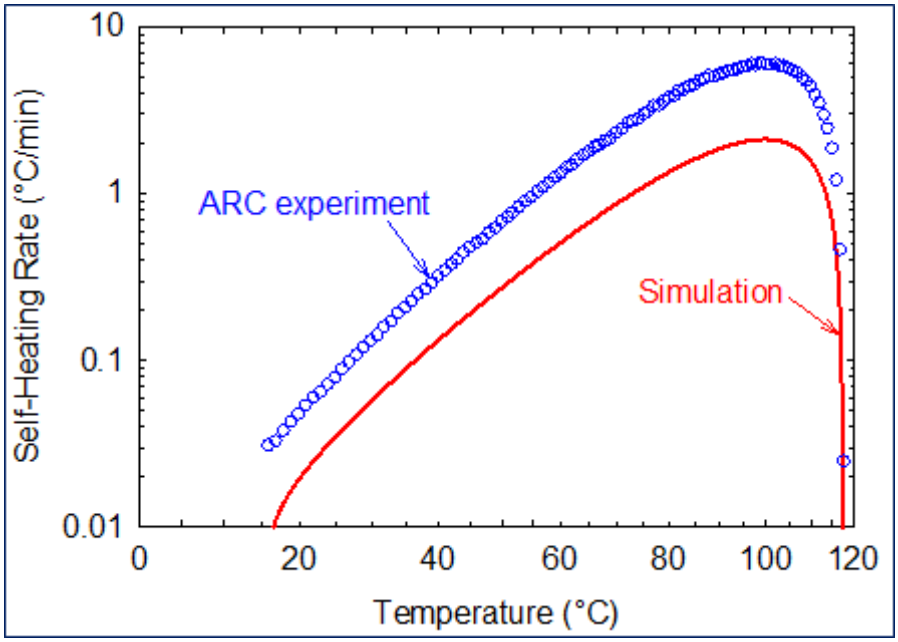

Figure 19: Linear-scale plot, experimental data and simulation with Bohms et al. [8] kinetic parameters

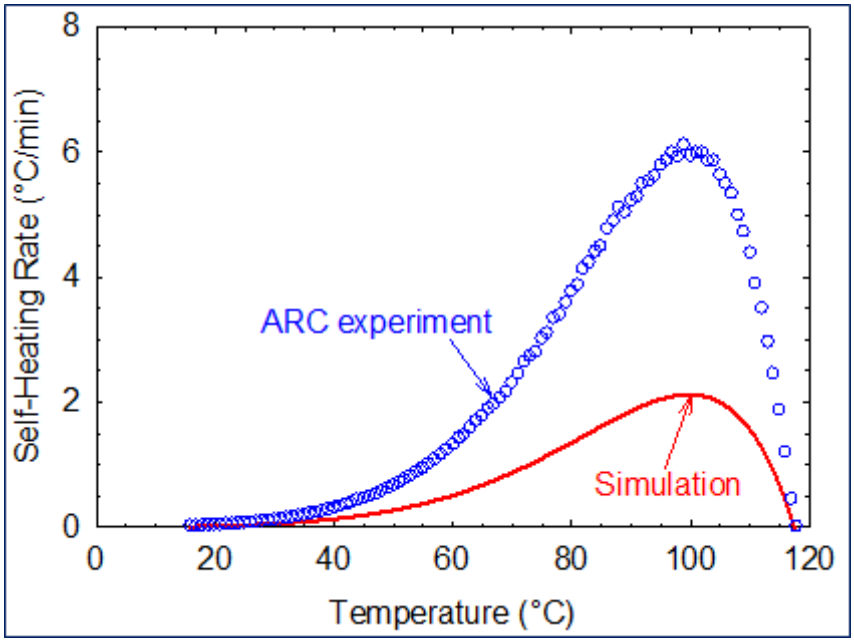


The Arrhenius plot in Figure 18 shows that the experimental and simulated data are close to parallel. This work can keep the same activation energies because of the nearly identical curve shapes. However, adjustments are needed for the pre-exponential factors $k_{o1}$' and $k_{o2}$', and the autocatalytic exponent j.

Some trial-and-error runs in SuperChems™ led to the following:

- $k_{o1}$' is in the range [$4x10^8$ to $8x10^8$]
- $k_{o2}$' is in the range [$4x10^5$ to $8x10^5$]
- j is in the range [0.25 to 0.35] (later found not to be the case)

Response Surface Methodology (RSM) with a Central Composite Design with three predictors will be used to find the optimum of $k_{o1}$', $k_{o2}$', and j. The design was modified with one central point instead of the standard model with six. The reason is that the "experiments" are dynamic simulations, and the results would be identical replicates with any number of runs with the same predictor values.

Four self-heating rate responses were considered in Approach 4: near the beginning of the runaway reaction (16.8 and 30.8°C), in the middle of the range (64.9°C), and at the peak

(98.8°C). The goal of the design is to develop a kinetic model that matches the following experimental self-heating rates as closely as possible:

- At 16.8°C: 0.033°C/min
- At 30.8°C: 0.143°C/min
- At 64.9°C: 1.789°C/min
- At 98.8°C: 6.125°C/min

It is virtually impossible to guess a combination of predictors in the design that yields close values to the experimental data. The statistical software applies an experimental design to find the best combination of predictors that closely match the targeted responses through desirability [7]. The Central Composite Design with three variables is shown in Figure 20:

Figure 20: First Central Composite Design with three variables for Approach 4

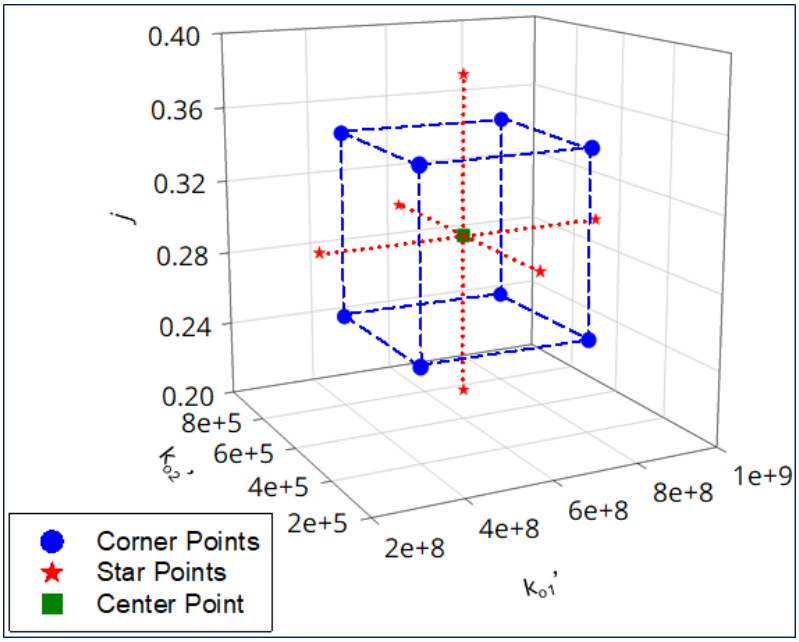


The simulation results are in Table 6:

Table 6: Simulations for the first design of Approach 4

| Run | $k_{o1}'$ | $k_{o2}'$ | $j$ | $T'$ at 16.8°C | $T'$ at 30.8°C | $T'$ at 64.9°C | $T'$ at 98.8°C | Type |
|---|---|---|---|---|---|---|---|---|
| 1 | 6.00E+08 | 936359 | 0.30000 | 0.03483 | 0.034834 | 0.190893 | 2.162710 | SP |
| 2 | 6.00E+08 | 600000 | 0.30000 | 0.02726 | 0.027260 | 0.142453 | 1.676020 | CtrP |
| 3 | 8.00E+08 | 400000 | 0.25000 | 0.03900 | 0.028744 | 0.132928 | 1.644980 | CP |
| 4 | 6.00E+08 | 263641 | 0.30000 | 0.01969 | 0.019686 | 0.094003 | 1.198440 | SP |
| 5 | 6.00E+08 | 600000 | 0.38409 | 0.02434 | 0.024336 | 0.140967 | 1.750780 | SP |
| 6 | 4.00E+08 | 400000 | 0.35000 | 0.01696 | 0.016958 | 0.094369 | 1.142630 | CP |
| 7 | 4.00E+08 | 800000 | 0.35000 | 0.02475 | 0.024749 | 0.151396 | 1.740610 | CP |
| 8 | 8.00E+08 | 400000 | 0.35000 | 0.02612 | 0.026123 | 0.131741 | 1.700490 | CP |
| 9 | 2.64E+08 | 600000 | 0.30000 | 0.01955 | 0.019553 | 0.111023 | 1.210670 | SP |
| 10 | 4.00E+08 | 400000 | 0.25000 | 0.01958 | 0.019579 | 0.095558 | 1.088460 | CP |
| 11 | 8.00E+08 | 800000 | 0.35000 | 0.03391 | 0.033914 | 0.188780 | 2.307280 | CP |
| 12 | 9.36E+08 | 600000 | 0.30000 | 0.03497 | 0.034967 | 0.173887 | 2.155170 | SP |
| 13 | 8.00E+08 | 800000 | 0.25000 | 0.03915 | 0.039155 | 0.191142 | 2.189490 | CP |
| 14 | 6.00E+08 | 600000 | 0.21591 | 0.03099 | 0.030990 | 0.143963 | 1.614110 | SP |
| 15 | 4.00E+08 | 800000 | 0.25000 | 0.02999 | 0.029990 | 0.153769 | 1.633670 | CP |

Predictors Responses

T' is the self-heating rate in °C/min. The design points are CP for the corner points, SP for the star points, CtrP for the center point, and EP for the extended point.

The design considered the following terms, but not all of them were statistically significant, as displayed in Table 7:

- Intercept (Constant)
- Linear terms: $k_{o1}'$, $k_{o2}'$, and j
- Square terms: $k_{o1}' * k_{o1}'$, $k_{o2}' * k_{o2}'$, and j * j
- Interaction terms: $k_{o1}' * k_{o2}'$, $k_{o1}' * j$ , and $k_{o2}' * j$

Table 7: Statistical analysis for each response of the first design of Approach 4

Estimated Regression Coefficients for dT/dt at 30.8°C

| Term | Coef | SE Coef | t | p |
|---|---|---|---|---|
| Constant | 0.027259 | 0.000011 | 2491.815 | 0.000 |
| ko1' | 0.007707 | 0.000013 | 575.766 | 0.000 |
| ko2' | 0.007620 | 0.000013 | 569.304 | 0.000 |
| j | -0.003314 | 0.000013 | -247.599 | 0.000 |
| j*j | 0.000403 | 0.000024 | 16.473 | 0.000 |
| ko2'*j | -0.001853 | 0.000029 | -62.991 | 0.000 |

S = 0.00002941 R-Sq = 100.0% R-Sq(adj) = 100.0%

Estimated Regression Coefficients for dT/dt at 30.8°C

| Term | Coef | SE Coef | t | p |
|---|---|---|---|---|
| Constant | 0.142454 | 0.000002 | 64825.168 | 0.000 |
| ko1' | 0.031430 | 0.000003 | 11689.196 | 0.000 |
| ko2' | 0.048451 | 0.000003 | 18019.515 | 0.000 |
| j | -0.001496 | 0.000003 | -556.503 | 0.000 |
| j*j | 0.000014 | 0.000005 | 2.785 | 0.021 |
| ko2'*j | -0.000834 | 0.000006 | -141.177 | 0.000 |

S = 0.000005908 R-Sq = 100.0% R-Sq(adj) = 100.0%

Estimated Regression Coefficients for dT/dt at 64.9°C

| Term | Coef | SE Coef | t | p |
|---|---|---|---|---|
| Constant | 1.68103 | 0.000749 | 2245.593 | 0.000 |
| ko1' | 0.47107 | 0.001319 | 357.028 | 0.000 |
| ko2' | 0.48227 | 0.001319 | 365.509 | 0.000 |
| j | 0.06949 | 0.001319 | 52.663 | 0.000 |
| ko2'*j | 0.04067 | 0.002899 | 14.028 | 0.000 |

S = 0.002899 R-Sq = 100.0% R-Sq(adj) = 100.0%

Estimated Regression Coefficients for dT/dt at 98.8°C

| Term | Coef | SE Coef | t | p |
|---|---|---|---|---|
| Constant | 5.79915 | 0.000857 | 6764.400 | 0.000 |
| ko1' | 1.98887 | 0.001049 | 1896.014 | 0.000 |
| ko2' | 1.26209 | 0.001049 | 1203.172 | 0.000 |
| j | 0.27105 | 0.001049 | 258.400 | 0.000 |
| j*j | 0.01477 | 0.001917 | 7.705 | 0.000 |
| ko2'*j | 0.15420 | 0.002305 | 66.900 | 0.000 |

S = 0.002305 R-Sq = 100.0% R-Sq(adj) = 100.0%

Analysis of Variance for dT/dt at 16.8°C

| Source | DF | Seq SS | Adj SS | Adj MS | F | p |
|---|---|---|---|---|---|---|
| Regression | 5 | 0.000624 | 0.000624 | 0.000125 | 144231.70 | 0.000 |
| Linear | 3 | 0.000620 | 0.000620 | 0.000207 | 238973.07 | 0.000 |
| Square | 1 | 0.000000 | 0.000000 | 0.000000 | 271.37 | 0.000 |
| Interaction | 1 | 0.000003 | 0.000003 | 0.000003 | 3967.89 | 0.000 |
| Residual Error | 9 | 0.000000 | 0.000000 | 0.000000 | | |
| Total | 14 | 0.000624 | | | | |

Analysis of Variance for dT/dt at 30.8°C

| Source | DF | Seq SS | Adj SS | Adj MS | F | p |
|---|---|---|---|---|---|---|
| Regression | 5 | 0.016116 | 0.016116 | 0.003223 | 92333972.97 | 0.000 |
| Linear | 3 | 0.016115 | 0.016115 | 0.005372 | 1.53883E+08 | 0.000 |
| Square | 1 | 0.000000 | 0.000000 | 0.000000 | 7.76 | 0.021 |
| Interaction | 1 | 0.000001 | 0.000001 | 0.000001 | 19930.89 | 0.000 |
| Residual Error | 9 | 0.000000 | 0.000000 | 0.000000 | | |
| Total | 14 | 0.016116 | | | | |

Analysis of Variance for dT/dt at 64.9°C

| Source | DF | Seq SS | Adj SS | Adj MS | F | p |
|---|---|---|---|---|---|---|
| Regression | 4 | 2.21944 | 2.21944 | 0.554861 | 66008.89 | 0.000 |
| Linear | 3 | 2.21779 | 2.21779 | 0.739263 | 87946.25 | 0.000 |
| Interaction | 1 | 0.00165 | 0.00165 | 0.001654 | 196.79 | 0.000 |
| Residual Error | 10 | 0.00008 | 0.00008 | 0.000008 | | |
| Total | 14 | 2.21953 | | | | |

Analysis of Variance for dT/dt at 98.8°C

| Source | DF | Seq SS | Adj SS | Adj MS | F | p |
|---|---|---|---|---|---|---|
| Regression | 5 | 27.1692 | 27.1692 | 5.43385 | 1022759.96 | 0.000 |
| Linear | 3 | 27.1451 | 27.1451 | 9.04838 | 1703088.26 | 0.000 |
| Square | 1 | 0.0003 | 0.0003 | 0.00032 | 59.37 | 0.000 |
| Interaction | 1 | 0.0238 | 0.0238 | 0.02378 | 4475.64 | 0.000 |
| Residual Error | 9 | 0.0000 | 0.0000 | 0.00001 | | |
| Total | 14 | 27.1693 | | | | |

Table 7 shows that the statistically significant terms are the following for the dT/dt responses:

- At 16.8, 30.8, and 98.8°C: Constant, $k_{o1}$', $k_{o2}$', j, j*j, and $k_{o2}$'*j, Intercept, linear terms, one quadratic term, and one interaction
- At 64.9°C: Constant, $k_{o1}$', $k_{o2}$', j, and $k_{o2}$'*j, Intercept, linear terms, and one interaction

The desirability function [7] was used for the optimization of parameters. The combined analysis including all parameters is displayed in Figure 21.

Figure 21: First design optimization for the predictors of Approach 4

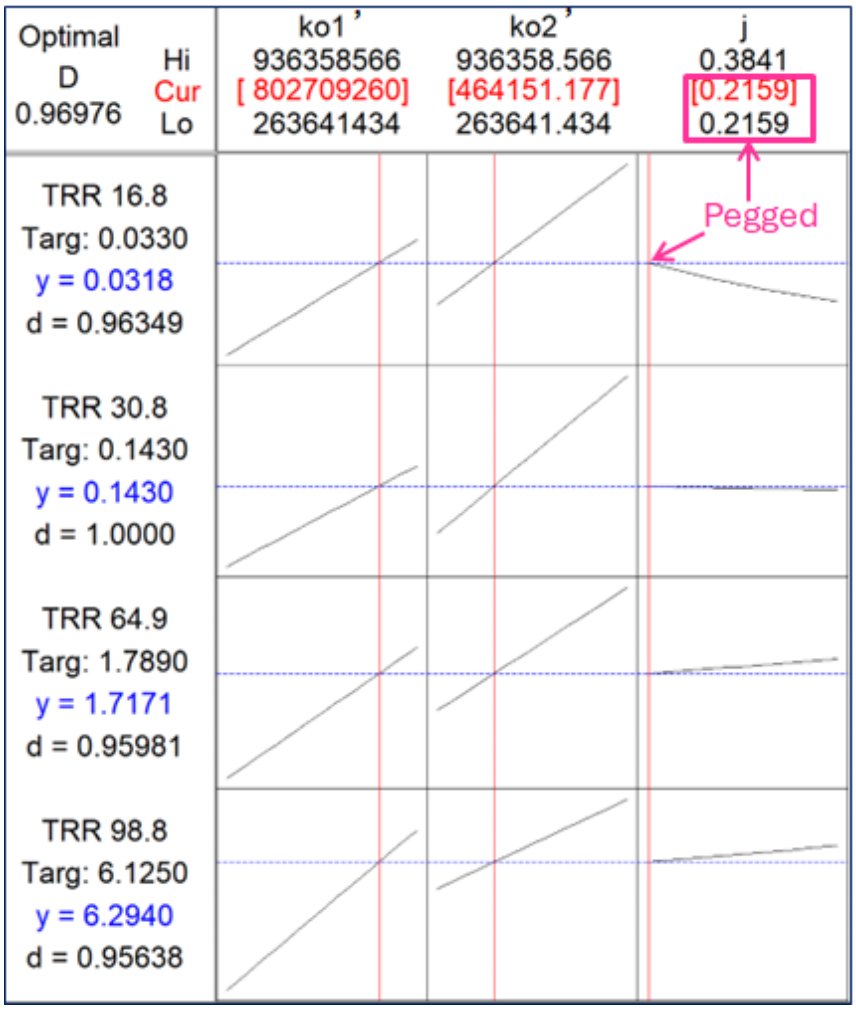

The optimal desirability D is the geometric mean of the individual desirability values d:

$$D = \sqrt[4]{d_1 d_2 d_3 d_4}$$
$$D = \sqrt[4]{(0.96349)(1.00000)(0.95981)(0.95638)}$$
$$D = 0.96976$$

Figure 21 shows red lines for the combined optima of self-heating rates at the four design temperatures. The design is quite good, given the individual desirability values. However, parameter j is pegged at the low end. This is undesirable because the optimum j is lower than the design calculated. The composite desirability D is quite good but can be improved if no parameter is pegged at one end.

Figure 21 indicates that j was overpredicted because the values chosen for the design were not sufficiently low to reach the optimum. Rather than adding an extra point, one of the corner points was modified to allow j to be in range. Figure 22 shows the modified design.

Figure 22: Second Central Composite Design with three variables for Approach 4

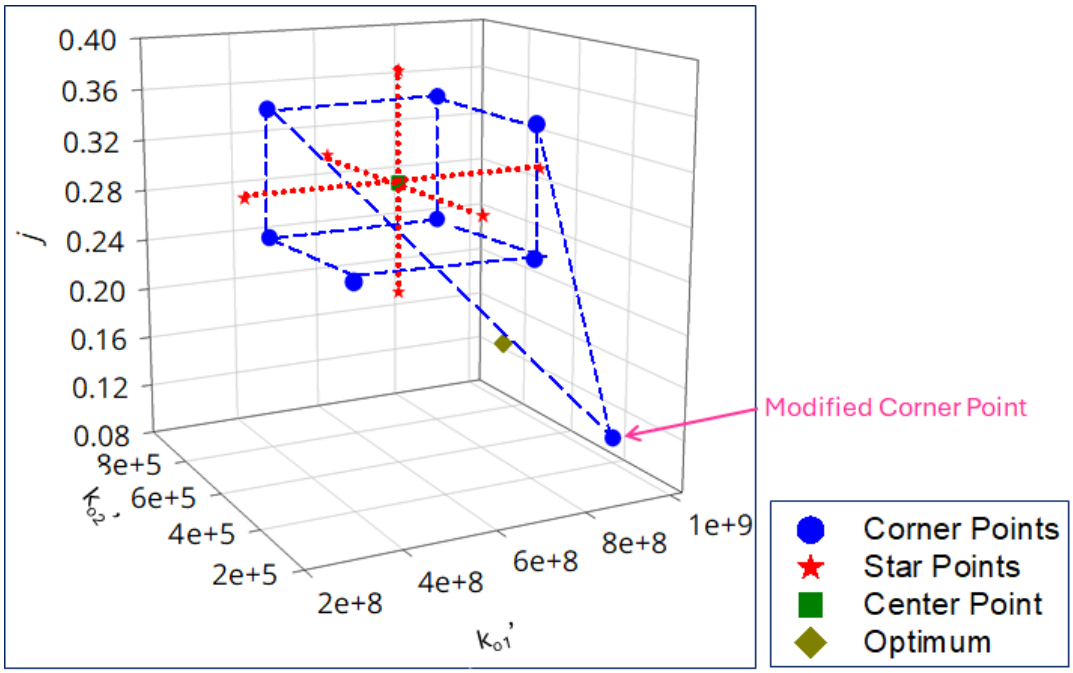


The simulation results for the second design of Approach 4 are in Table 8.

Table 8: Simulations for the second design of Approach 4. The modified corner point is in red.

| Run | $k_{o1}'$ | $k_{o2}'$ | $j$ | $T'$ at 16.8°C | $T'$ at 30.8°C | $T'$ at 64.9°C | $T'$ at 98.8°C | Type |
|---|---|---|---|---|---|---|---|---|
| 1 | 6.00E+08 | 936359 | 0.30000 | 0.03483 | 0.034834 | 0.190893 | 2.162710 | SP |
| 2 | 6.00E+08 | 600000 | 0.30000 | 0.02726 | 0.027260 | 0.142453 | 1.676020 | CtrP |
| 3 | 1.00E+09 | 400000 | 0.10000 | 0.03900 | 0.153439 | 1.855340 | 7.049450 | MCP |
| 4 | 6.00E+08 | 263641 | 0.30000 | 0.01969 | 0.019686 | 0.094003 | 1.198440 | SP |
| 5 | 6.00E+08 | 600000 | 0.38409 | 0.02434 | 0.024336 | 0.140967 | 1.750780 | SP |
| 6 | 4.00E+08 | 400000 | 0.35000 | 0.01696 | 0.016958 | 0.094369 | 1.142630 | CP |
| 7 | 4.00E+08 | 800000 | 0.35000 | 0.02475 | 0.024749 | 0.151396 | 1.740610 | CP |
| 8 | 8.00E+08 | 400000 | 0.35000 | 0.02612 | 0.026123 | 0.131741 | 1.700490 | CP |
| 9 | 2.64E+08 | 600000 | 0.30000 | 0.01955 | 0.019553 | 0.111023 | 1.210670 | SP |
| 10 | 4.00E+08 | 400000 | 0.25000 | 0.01958 | 0.019579 | 0.095558 | 1.088460 | CP |
| 11 | 8.00E+08 | 800000 | 0.35000 | 0.03391 | 0.033914 | 0.188780 | 2.307280 | CP |
| 12 | 9.36E+08 | 600000 | 0.30000 | 0.03497 | 0.034967 | 0.173887 | 2.155170 | SP |
| 13 | 8.00E+08 | 800000 | 0.25000 | 0.03915 | 0.039155 | 0.191142 | 2.189490 | CP |
| 14 | 6.00E+08 | 600000 | 0.21591 | 0.03099 | 0.030990 | 0.143963 | 1.614110 | SP |
| 15 | 4.00E+08 | 800000 | 0.25000 | 0.02999 | 0.029990 | 0.153769 | 1.633670 | CP |

Predictors Responses

T' is the self-heating rate in °C/min. The design points are CtrP for the central point, CP for the corner points, MCP for the modified corner point in red, and SP for the star points. The corresponding statistical analysis is in Table 9.

Table 9: Statistical analysis for each response of the second design of Approach 4

Estimated Regression Coefficients for dT/dt at 30.8°C

| Term | Coef | SE Coef | t | p |
|---|---|---|---|---|
| Constant | 0.030447 | 0.000017 | 1809.731 | 0.000 |
| ko1' | 0.008432 | 0.000022 | 391.789 | 0.000 |
| ko2 | 0.008915 | 0.000037 | 242.239 | 0.000 |
| j | -0.006367 | 0.000036 | -176.886 | 0.000 |
| j*j | 0.000959 | 0.000049 | 19.572 | 0.000 |
| ko2'*j | -0.003170 | 0.000072 | -44.214 | 0.000 |

S = 0.00004157 R-Sq = 100.0% R-Sq(adj) = 100.0%

Estimated Regression Coefficients for dT/dt at 30.8°C

| Term | Coef | SE Coef | t | p |
|---|---|---|---|---|
| Constant | 0.146464 | 0.000003 | 56934.368 | 0.000 |
| ko1' | 0.034403 | 0.000003 | 10454.680 | 0.000 |
| ko2' | 0.049026 | 0.000006 | 8711.876 | 0.000 |
| j | -0.002544 | 0.000006 | -462.161 | 0.000 |
| j*j | 0.000020 | 0.000007 | 2.717 | 0.024 |
| ko2'*j | -0.001411 | 0.000011 | -128.686 | 0.000 |

S = 0.000006357 R-Sq = 100.0% R-Sq(adj) = 100.0%

Estimated Regression Coefficients for dT/dt at 64.9°C

| Term | Coef | SE Coef | t | p |
|---|---|---|---|---|
| Constant | 1.67884 | 0.001001 | 1676.398 | 0.000 |
| ko1' | 0.51653 | 0.001349 | 382.997 | 0.000 |
| ko2' | 0.45160 | 0.001821 | 248.037 | 0.000 |
| j | 0.11575 | 0.001834 | 63.127 | 0.000 |
| ko2'*j | 0.07337 | 0.003510 | 20.899 | 0.000 |

S = 0.002762 R-Sq = 100.0% R-Sq(adj) = 100.0%

Estimated Regression Coefficients for dT/dt at 98.8°C

| Term | Coef | SE Coef | t | p |
|---|---|---|---|---|
| Constant | 5.80601 | 0.000939 | 6181.996 | 0.00 |
| ko1' | 2.17614 | 0.001201 | 1811.351 | 0.000 |
| ko2' | 1.15844 | 0.002055 | 563.850 | 0.000 |
| j | 0.43068 | 0.002009 | 214.342 | 0.000 |
| j*j | 0.03530 | 0.002735 | 12.905 | 0.000 |
| ko2'*j | 0.25584 | 0.004002 | 63.924 | 0.000 |

S = 0.002321 R-Sq = 100.0% R-Sq(adj) = 100.0%

Analysis of Variance for dT/dt at 16.8°C

| Source | DF | Seq SS | Adj SS | Adj MS | F | p |
|---|---|---|---|---|---|---|
| Regression | 5 | 0.000750 | 0.000750 | 0.000150 | 86771.49 | 0.000 |
| Linear | 3 | 0.000746 | 0.000454 | 0.000151 | 87550.84 | 0.000 |
| Square | 1 | 0.000000 | 0.000001 | 0.000001 | 383.07 | 0.000 |
| Interaction | 1 | 0.000003 | 0.000003 | 0.000003 | 1954.88 | 0.000 |
| Residual Error | 9 | 0.000000 | 0.000000 | 0.000000 | | |
| Total | 14 | 0.000750 | | | | |

Analysis of Variance for dT/dt at 30.8°C

| Source | DF | Seq SS | Adj SS | Adj MS | F | p |
|---|---|---|---|---|---|---|
| Regression | 5 | 0.016118 | 0.016118 | 0.003224 | 79773461.74 | 0.000 |
| Linear | 3 | 0.016116 | 0.008922 | 0.002974 | 73596235.51 | 0.000 |
| Square | 1 | 0.000001 | 0.000000 | 0.000000 | 7.38 | 0.024 |
| Interaction | 1 | 0.000001 | 0.000001 | 0.000001 | 16560.18 | 0.000 |
| Residual Error | 9 | 0.000000 | 0.000000 | 0.000000 | | |
| Total | 14 | 0.016118 | | | | |

Analysis of Variance for dT/dt at 64.9°C

| Source | DF | Seq SS | Adj SS | Adj MS | F | p |
|---|---|---|---|---|---|---|
| Regression | 4 | 2.24558 | 2.24558 | 0.561396 | 73600.63 | 0.000 |
| Linear | 3 | 2.24225 | 1.47540 | 0.491801 | 64476.55 | 0.000 |
| Interaction | 1 | 0.00333 | 0.00333 | 0.003331 | 436.77 | 0.000 |
| Residual Error | 10 | 0.00008 | 0.00008 | 0.000008 | | |
| Total | 14 | 2.24566 | | | | |

Analysis of Variance for dT/dt at 98.8°C

| Source | DF | Seq SS | Adj SS | Adj MS | F | p |
|---|---|---|---|---|---|---|
| Regression | 5 | 28.5567 | 28.5567 | 5.71135 | 1060422.93 | 0.000 |
| Linear | 3 | 28.5035 | 20.9075 | 6.96916 | 1293960.29 | 0.000 |
| Square | 1 | 0.0312 | 0.0009 | 0.00090 | 166.54 | 0.000 |
| Interaction | 1 | 0.0220 | 0.0220 | 0.02201 | 4086.22 | 0.000 |
| Residual Error | 9 | 0.0000 | 0.0000 | 0.00001 | | |
| Total | 14 | 28.5568 | | | | |

Table 7 and 9 show the same statistically significant terms in the first and second designs. The desirability analysis of the second design of Approach 4 is displayed in Figure 23.

Figure 23: Second design optimization for the predictors of Approach 4

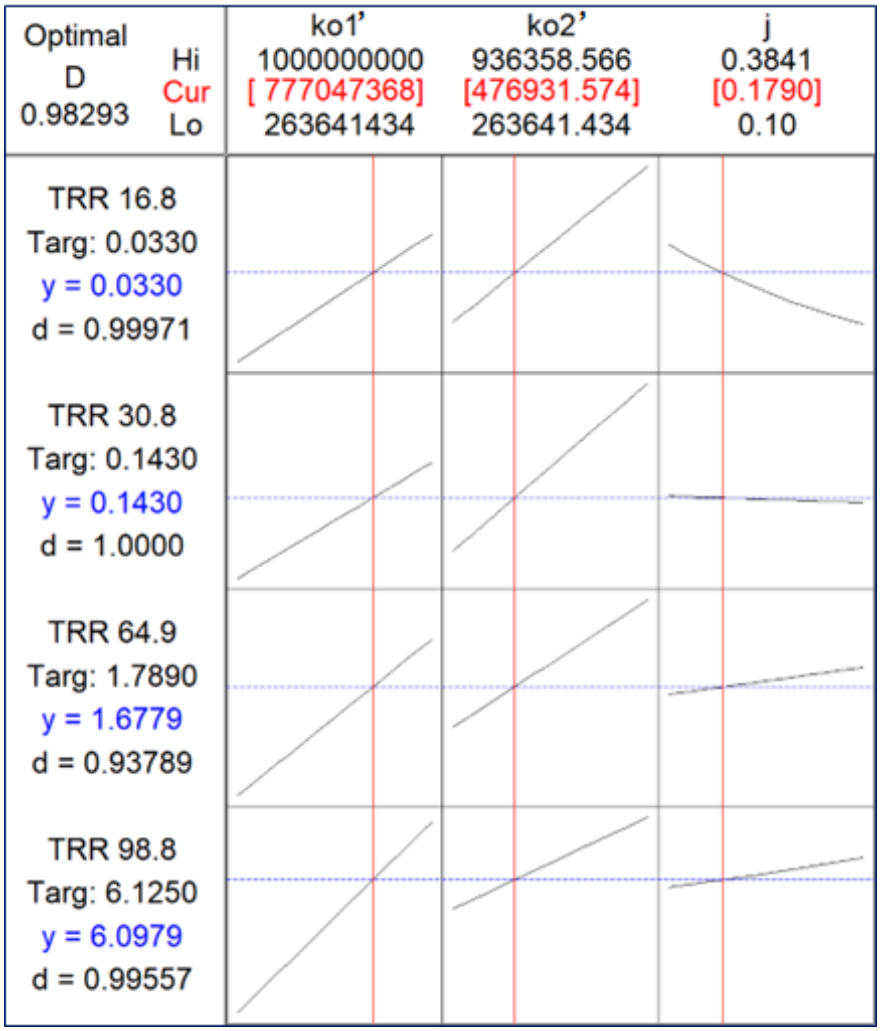


As calculated before, the optimal desirability D is the geometric mean of the individual desirability values d:

$$D = \sqrt[4]{d_1 d_2 d_3 d_4}$$
$$D = \sqrt[4]{(0.99971)(1.00000)(0.93789)(0.99557)}$$
$$D = 0.98293$$

Figure 23 shows red lines for the combined optima of self-heating rates at the four design temperatures. All the predictors, $k_{o1}$', $k_{o2}$', and j, are within their design limits, so none is pegged at one end of their respective ranges.

Instead of one contour plot as in Figure 15 of Approach 3 with two predictors, there are three contour plots in Figure 24 of Approach 4 with three predictors.

Figure 24: Overlaid contour plots for the second design of Approach 4

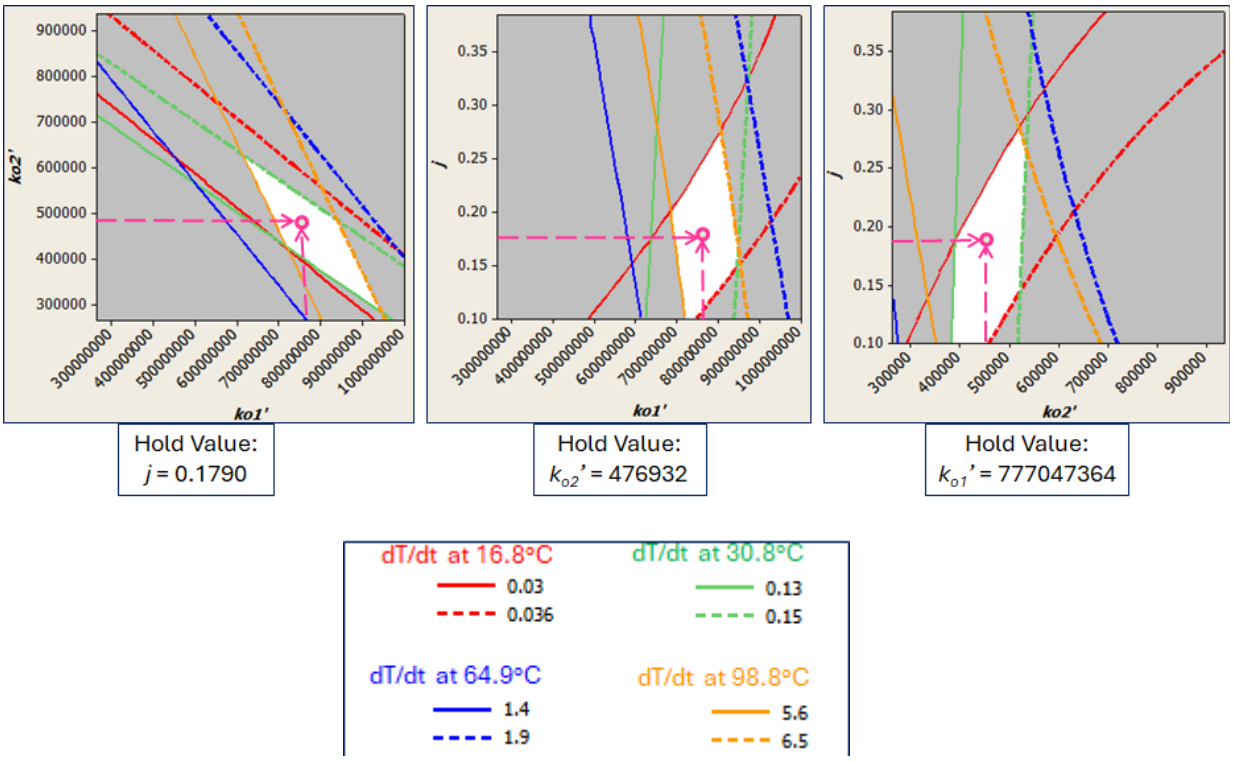


The hold values and the dots are at the optimum of the design. The white zones represent the feasibility regions for the optimum. The curvatures in the graph lines are due to statistically significant quadratic and interaction terms.

From the input data and desirability plot, the following optimized values are obtained for the predictors, in proper units, per Equation (14):

$$k_{o1}' = 777047368 \frac{m^3}{kg\text{-}mol.s}$$

$$B_1 = 10339\,K$$

$$k_{o2}' = 476932 \left( \frac{m^3}{kg\text{-}mol.s} \right)^{1.1790}$$

$$B_2 = 8089$$

$$j = 0.1790$$

Figure 25 shows a reverse Arrhenius plot of the experimental data and simulation with the optimized parameters of Approach 4.

Figure 25: Comparison of the Approach 4 model with experimental data on a reverse Arrhenius scale

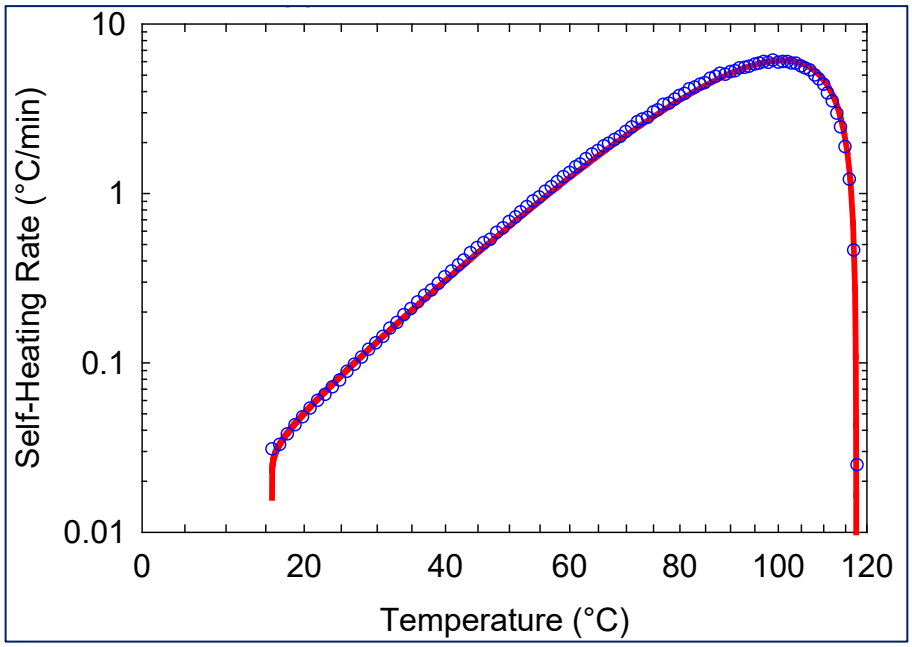


As in Approach 3, the steep rise in the simulated self-heating rate at the onset of the exotherm observed in Figure 25 is characteristic of autocatalysis. See Figure 2. The experiment could not register this sudden self-heating rate of rise due to the ARC's limited measurement capabilities below 0.02°C/min. Figure 26 exhibits the same data in a plot with linear coordinates for completeness. The match is good, as in Approach 3.

Figure 26: Comparison of the Approach 4 model with experimental data on a linear scale

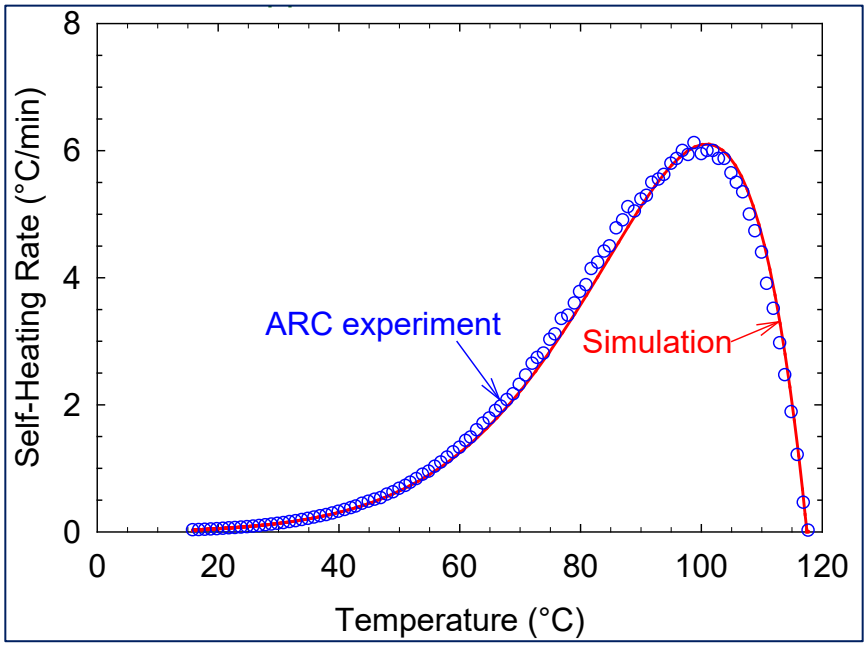


For Approach 4 it is desired to compare the two reaction rates, i.e., with and without autocatalysis (AC). The AC ratio is sought along the exotherm.

$$AC = \frac{\text{Autocatalysis Rate}}{\text{Non-Autocatalysis Rate + Autocatalysis Rate}}$$

In kinetic rate format:

$$AC = \frac{k'_{02} e^{-\frac{B_2}{T}} C_a C_m C_c^j}{k'_{01} e^{-\frac{B_1}{T}} C_a C_m + k'_{02} e^{-\frac{B_2}{T}} C_a C_m C_c^j} \tag{41}$$

Equation (41) is plotted in Figure27 based on a SuperChems™ simulation with the optimum values of the predictors of Approach 4.

Figure 27: Autocatalysis effect in Approach 4: Equation (41) vs. temperature

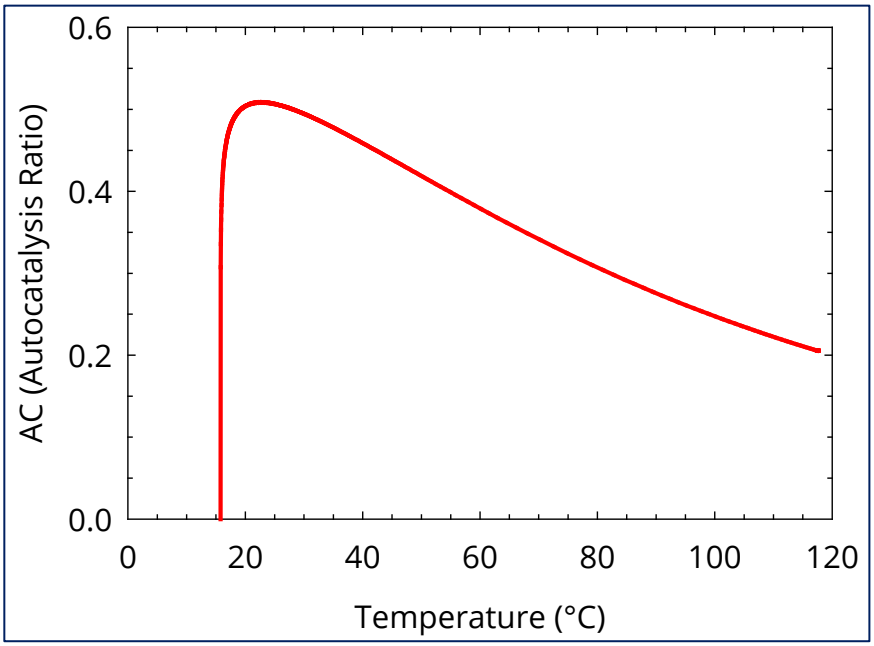


According to Figure 27, the autocatalytic effect peaks soon after the onset of the exotherm and tapers down as the runaway reaction progresses. The non-autocatalytic reaction has higher activation energy ($B_1$), so it grows faster than the autocatalytic reaction as the temperature rises.

# Additional Information

## Reaction Enthalpies

The reaction enthalpies used in the simulations were obtained as the sums of the formation enthalpies of products minus the sum of the formation enthalpies of the reactants as shown in Table 10. Formation enthalpies can be obtained from NIST at https://webbook.nist.gov/chemistry/ [9] upon searching for Thermophysical Properties of Fluid Systems for specific compounds.

Table 10: Enthalpies of formation for the compounds in this study

| Compound | Enthalpy of Formation (kJ/g-mol) | $M_w$ (g/g-mol) |
|---|---|---|
| Acetic Anhydride | -625.0 | 102.090 |
| Methanol | -238.9 | 32.042 |
| Methyl Acetate | -445.9 | 74.079 |
| Acetic Acid | -483.5 | 60.053 |

The enthalpy of formation based on NIST is then: (-445.9-483.5)-(-625.0-238.9) = -65.5 kJ/g-mol. However, the heats of reaction used in SuperChems™ calculations require some manipulations, as they are based on energy per unit mass.

Without autocatalysis: Approaches 1, 2, and the first reaction of Approach 4:

- -65.5 (kJ/g-mol)/(102.090+32.042) (g/g-mol) = -0.488 kJ/g = -0.488 MJ/kg
- What works best in SuperChems™: -0.48 MJ/kg, which is very close to the NIST value

With autocatalysis: Approach 3 and the second reaction of Approach 4:

- -65.5 (kg/g-mol)/(102.090+32.042+60.053) (g/g-mol) = -0.337 kJ/g = -0.337 MJ/kg
- What works best in SuperChems™: -0.33 MJ/kg, which is very close to the NIST value

The conclusion is that the reaction enthalpies based on formation energies coincide with values best suited for dynamic simulations.

## The $\phi$ -Factor Effect

Comparisons will be made next for the different approaches of this document:

- Self-heating rates at $\phi$ = 1.65 in Figure28
- Self-heating rates at $\phi$ = 1.00 in Figure 29

Figure 28: Self-heating rates for the four approaches at $\phi$ = 1.65

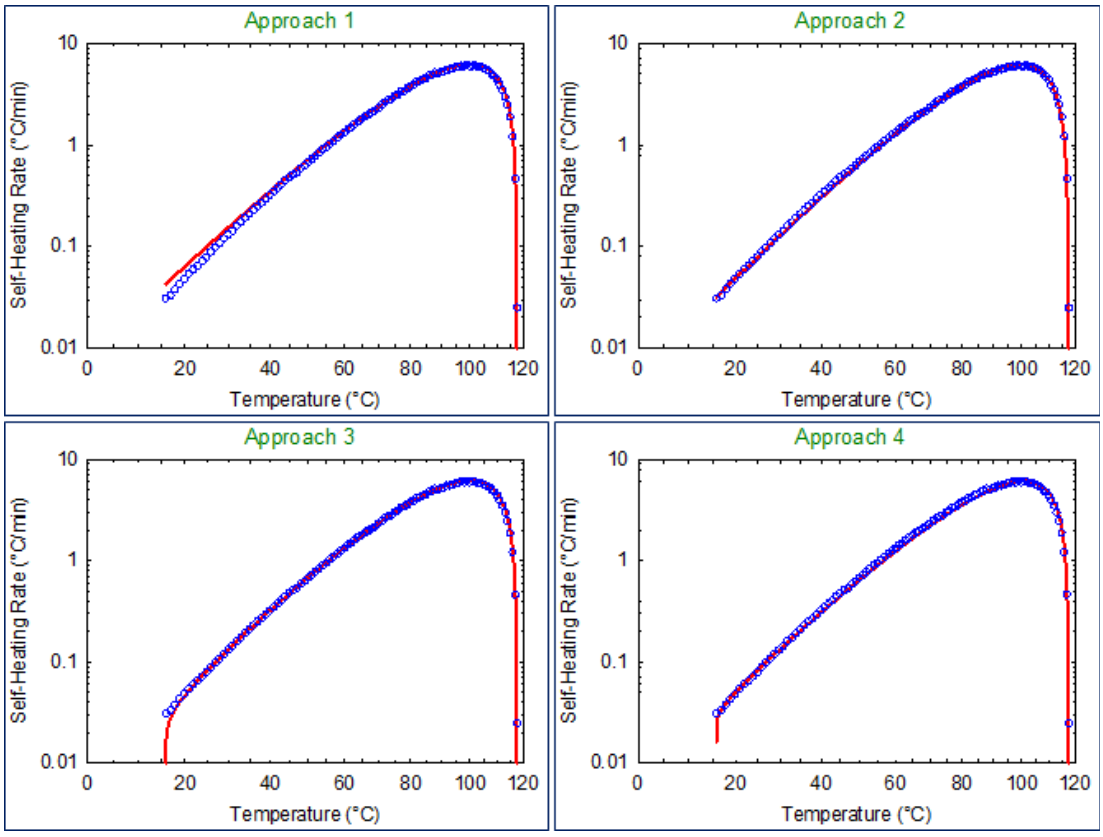


Approach 1 disregarded the autocatalytic effect of acetic acid. It shows a discrepancy in self-heating rates at lower temperatures. The self-heating rates for the four approaches at $\phi$ = 1 are plotted in Figure 29.

Figure 29: Self-heating rates for the four approaches at $\phi = 1$

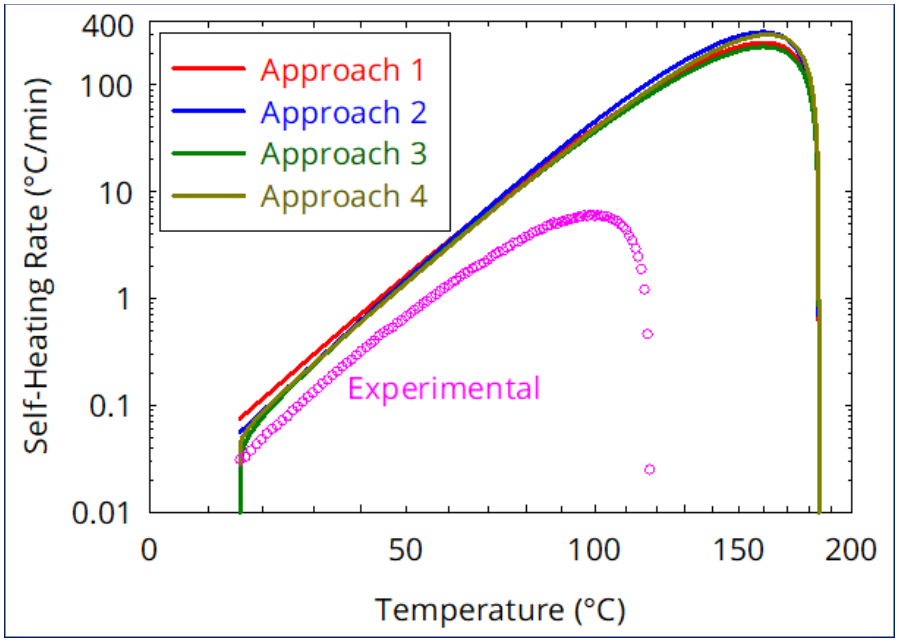


## Self-Pressurization Rate

The match of calculated self-pressurization rates with experimental data requires adequate BIPs. The BIPs in Table 11 were extracted from the SuperChems™ database, with one change: The BIP between methyl acetate and methanol was positive but turned negative with the same numerical value for better pressure agreement between simulations and the experiment.

Table 11: Binary Interaction Parameters (BIPs)

| $K_{ij}$ | Acetic Anhydride | Methanol | Methyl Acetate | Acetic Acid | Nitrogen |
|---|---|---|---|---|---|
| Acetic Anhydride | 0 | 0 | 0 | -0.01175 | 0 |
| Methanol | 0 | 0 | -0.02399 | -0.02974 | 0 |
| Methyl Acetate | 0 | -0.02399 | 0 | 0 | 0 |
| Acetic Acid | -0.01175 | -0.02974 | 0 | 0 | 0 |
| Nitrogen | 0 | 0 | 0 | 0 | 0 |

$K_{ij} = K_{ji}$ and $L_{ij} = -L_{ji} = 0$

BIPS System Pressure Basis: 101325 Pa

BIPS System Temperature Basis. 25°C

Figure 30 exhibits the self-pressurization rates for the four approaches. It shows that Approaches 2, 3, and 4 have virtually identical self-pressurization rates throughout. Approach 1 has higher rates at lower temperatures because the self-heating rates are higher, as autocatalysis was not considered.

Figure 30: Self-pressurization rates for the four approaches at $\phi = 1.65$

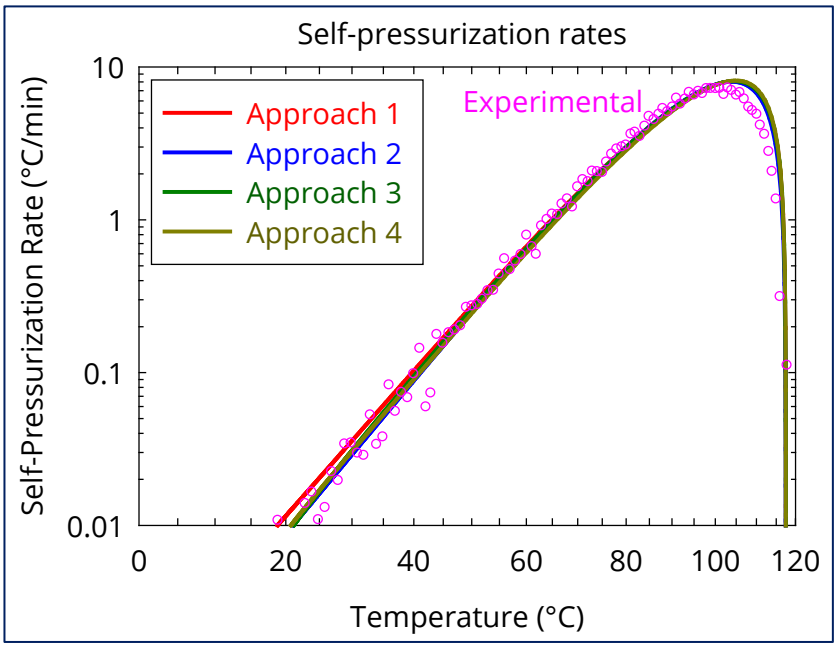


Figure 31 demonstrates that Approach 1 has a faster pressure build-up because autocatalysis is not considered, so the reaction is quick at the onset. The only difference between the curves is the time to reach the peak pressure, as Figure 31 shows.

Figure 31: Simulations based on a sealed ARC for the four kinetic approaches

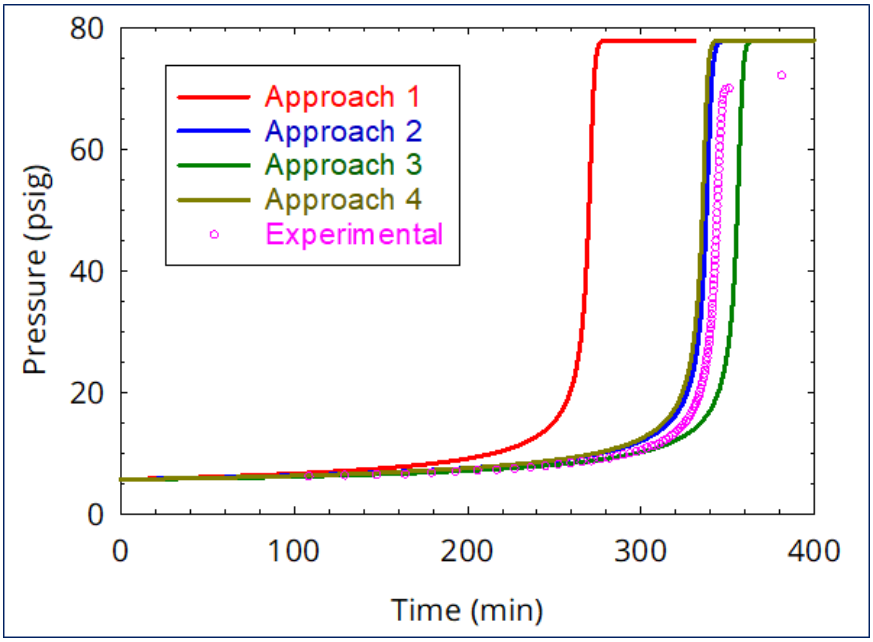

A 44-minute time simulation offset was applied to all approaches to account for delays at the beginning of the experiment. Some delays include:

- Calorimeter self-checks after the experiment initiates
- Heat-wait-search routine to detect the onset of the exotherm

More important than the numerical value of the offset is the match between the experiment and simulation curve shapes in Figures 30 and 31.

## Conclusions

Four kinetic approaches for the reaction of acetic anhydride with methanol were considered for SuperChems™ simulations in this study:

- Approach 1: Single reaction, no autocatalysis
- Approach 2: Single reaction, adjusting the reaction order to emulate autocatalysis
- Approach 3: Single reaction with autocatalysis
- Approach 4: Two reactions, one with and one without autocatalysis

Approaches 1 and 2 were developed with graphs, spreadsheets, and simple statistics for one predictor (pre-exponential factor). Approaches 3 and 4 required advanced statistics for multiple predictors. The chosen method was Response Surface Methodology (RSM) with a Central Composite Design. The “experiments” are SuperChems™ dynamic simulations of a sealed adiabatic calorimeter. It is virtually impossible to optimize multiple kinetic parameters concurrently by trial and error. RSM is a systematic approach to optimizing two or more predictors.

The experiment could not capture the autocatalytic effect of acetic acid because its detection limit is 0.02°C/min. Most of the autocatalysis onset takes place below 0.02°C/min. SuperChems™ dynamic simulations with Approaches 3 and 4 portrayed the onset of autocatalysis.

The shapes of the curves for all approaches are similar. From a timing perspective, it takes longer to reach the peak exotherm with models developed with autocatalysis due to the slow beginning of the chemical reaction.

This white paper demonstrated the benefits of using RSM to develop kinetic parameters. Autocatalysis is not necessary for the application of RSM. Indeed, any parameters can be used as predictors: activation energy, pre-exponential factor, order of each reactant, BIPs, and many others. However, it is necessary to be sensitive to the fact that the number of experiments, that is, SuperChems™ runs, grows substantially with the number of predictors. It becomes increasingly cumbersome to apply RSM for many predictors.

## Author

1. Enio Kumpinsky; kumpinsky.e.nh@ioMosaic.com

## Figure Sources

Figures 1-9, 16-19, 25-31: SigmaPlot® Scientific Graphing and Statistics Software

Figures 10-15, 20-24: Minitab® Statistics Software

## Nomenclature

| | |
|---|---|
| ARC | Accelerating Rate Calorimeter |
| B | Activation energy divided by the universal gas constant (E/R) |
| BIPs | Binary Interaction Parameters |
| C | Concentration |
| $C_a$ | Concentration of acetic anhydride |
| $C_{ao}$ | Initial concentration of acetic anhydride |
| $C_m$ | Concentration of methanol |
| $C_c$ | Concentration of acetic acid |
| CCD | Central Composite Design |
| DIERS | Design Institute for Emergency Relief Systems |
| E | Activation energy |
| k’ | Kinetic constant adjusted for dynamic simulations |
| k | Lumped kinetic constant, calorimetry |
| $k_o$ | Pre-exponential factor |
| $k_o$’ | Pre-exponential factor adjusted for dynamic simulations |
| m | Order of reaction, methanol |
| n | Order of reaction, acetic anhydride |
| j | Order of reaction, acetic acid in autocatalysis |
| R | Universal gas constant or Pearson correlation coefficient |

| | |
|---|---|
| RSM technique | Response Surface Methodology, an experimental design |
| t | Time |
| T | Temperature |
| $T_o$ | Onset temperature of a runaway reaction |
| $T_f$ | Final temperature of a runaway reaction |
| X | Conversion of acetic anhydride |
| $\Delta H$ | Enthalpy of chemical reaction |
| $\Delta T_a$ | Adiabatic temperature rise, $T_f - T_o$ |

## Additional ioMosaic White Paper Resources

It is impossible to cover all aspects and facets of chemical reactivity management in one white paper. The resources provided below address in more detail several key topics and can be requested from sales@iomosaic.com or melhem@iomosaic.com:

### Chemical Reactivity Management

1. Systematic Evaluation of Chemical Reaction Hazards
2. Quickly Develop Chemical Interaction Matrices with SuperChems™
3. Thermal Stability Indicators
4. Calculate Phase and Chemical Equilibria Using Process Safety Office SuperChems™
5. An Advanced Method for the Estimation of Reaction Stoichiometry and Rates from ARC Data
6. Development of Kinetic Models - Part I. Thermal Stability
7. Development of Kinetic Models - Part II. Pressure Relief Systems
8. Forget direct scaleup vent sizing and master kinetic modeling instead
9. Polymerization Modeling for Emergency Relief Systems
10. Polymerization Reactions Inhibitor Modeling - Styrene and Butyl Acrylate Incidents Case Studies
11. Polymerization Models for butadiene, vinyl acetate, acrylates, acrylonitrile, and isoprene

### Fire Modeling

2. Fire Exposure Modeling Considerations
3. RAGAGEP Considerations for Overtemperature Protection in Relief Systems

### Pressure Relief and Vent Containment Design

1. Two-phase Flow Onset and Disengagement Methods
2. Vent Containment Design For Emergency Relief Systems
3. Forget the Omega Method and Master vdP Integration Instead
4. Advanced Pressure Relief Design Using Computer Simulation
5. Beware of Temperature Increase During Rapid Vessel Charging
6. Heat of vaporization considerations for relief systems applications
7. Properly Calculate Relief Systems Reaction Forces

8. Realize Better Risk Characterization of STHE Tube Failure Scenarios Through Relief Systems Dynamics Modeling
9. Relief and Flare Systems Statics vs Dynamics
10. Relief Requirements for Distillation Columns
11. Retrograde and Phase Change (RPC) Flow Considerations for Relief and Depressuring Systems
12. Retrograde and Phase Change (RPC) Flow Considerations for Relief and Flare Systems
13. Single and Multiphase Control Valve Flow
14. The Anatomy of Liquid Displacement and High-Pressure Fluid Breakthrough
15. Thermal Expansion Relief Requirements for Liquids, Vapors, and Supercritical Fluids
16. Quantify Non-Equilibrium Flow and Rapid Phase Transitions

## PRV Stability

1. Analysis of PRV Stability In Relief Systems - Detailed Dynamics - Part I
2. Analysis of PRV Stability In Relief Systems - Screening - Part II
3. Analysis of PRV Stability In Relief Systems - How to Avoid the Singing PRV Problem - Part III
4. Analysis of PRV Stability In Relief Systems - On the Estimation of Speed of Sound - Part IV
5. Analysis of PRV Stability In Relief Systems - Get a Handle on PRV Stability - Part V
6. PRV stability inlet line critical length
7. PRV Stability - Bridging the 3 percent pressure loss rule gap

## Fire and Explosion Modeling

1. Calculate Flammability Limits Using Process Safety Office® SuperChems™
2. How Flame Arresters Work
3. Development of Reduced Analytical Models for Explosion Dynamics
4. Quantify Explosion Venting Dynamics in Vessels Enclosures and Energy Storage Systems

## Process Safety Management and Automation

1. Effectively Manage Mechanical Integrity in Process Safety Enterprise®
2. Effectively Manage Changes to Processes, Chemicals, Equipment, and Personnel Using Process Safety Enterprise®
3. Properly Evaluate Building and Facility Siting Risks
4. Emergency Response and Process Hazard Analysis Charts
5. Usage of AEGL Dosage in Safety and Risk Studies
6. Driving Safety and Business Performance Through Data Mining

## References


[1] Response Surface Designs. NIST Engineering Statistics Handbook, 5.3.3.6, National Institute of Standards and Technology at the U.S. Department of Commerce.

[2] Central Composite Design. NIST Engineering Statistics Handbook, 5.3.3.6.1, National Institute of Standards and Technology at the U.S. Department of Commerce.

[3] George Box, J. Stuart Hunter, and William G. Hunter. Statistics for Experimenters. Wiley-Interscience, Second Edition (May 1, 2005).

[4] Mark J. Kiemele, Stephen R. Schmidt, and Ronald J. Berdine. Basic Statistics: Tools for Continuous Improvement. Air Academy Press, Fourth Edition (January 1, 1997).

[5] Douglas C. Montgomery, George C. Hunger, and Norma F. Hubele. Engineering Statistics. John Wiley & Sons; 5th edition (December 21, 2010).

[6] Murray R. Spiegel and Larry J. Stephens. Schaum's Outline of Statistics. McGraw Hill, Sixth Edition (October 26, 2017).

[7] Multiple responses: The desirability approach. NIST Engineering Statistics Handbook, 5.5.3.2.2, National Institute of Standards and Technology at the U.S. Department of Commerce.

[8] Stefan Bohm, Günther Hessel, Holger Kryk, Horst-Michael Prasser, and Wilfried Schmitt. *Auto-Catalytic Effect of Acetic Acid on the Kinetics of the Methanol / Acetic Anhydride Esterification*. Paper in the 2004 Annual Report, Scientific and Technical Report FZR-420, pp. 53-58. Forschungszentrum Rossendorf, published in 2005. https://www.hzdr.de/FWS/publikat/JB04/JB_04_R09.pdf

[9] Thermophysical Properties of Fluid Systems at https://webbook.nist.gov/chemistry/